Research Square

Preprints are preliminary reports that have not undergone peer review.
They should not be considered conclusive, used to inform clinical practice,
or referenced by the media as validated information.

Functional characterization of the human Dicer1e isoform reveals non-canonical RNA processing and context-dependent remodeling of cellular regulatory networks

Marta Wojnicka
Institute of Bioorganic Chemistry, Polish Academy of Sciences
Arkadiusz Kajdasz
Institute of Bioorganic Chemistry, Polish Academy of Sciences
Lukasz Marczak
Institute of Bioorganic Chemistry, Polish Academy of Sciences
Piotr H. Malecki
Institute of Bioorganic Chemistry, Polish Academy of Sciences
Aleksander Strugala
Institute of Bioorganic Chemistry, Polish Academy of Sciences
Klaudia Wojcik
Institute of Bioorganic Chemistry, Polish Academy of Sciences
Konrad Kuczynski
Institute of Bioorganic Chemistry, Polish Academy of Sciences
Anna Philips
Institute of Bioorganic Chemistry, Polish Academy of Sciences
Anna Kurzynska-Kokorniak
akurzyns@man.poznan.pl

Institute of Bioorganic Chemistry, Polish Academy of Sciences

Research Article

Keywords: Dicer1e, human Dicer, transcript isoforms, RNase III, RNA cleavage, miRNA, transcriptomics, proteomics, cell proliferation

Posted Date: July 23rd, 2026

DOI: https://doi.org/10.21203/rs.3.rs-10281152/v1

License: This work is licensed under a Creative Commons Attribution 4.0 International License.
Read Full License

Additional Declarations: No competing interests reported.

Full Title:

Functional characterization of the human Dicer1e isoform reveals non-canonical RNA processing and context-dependent remodeling of cellular regulatory networks

Short Running Title:

Beyond miRNA biogenesis: Dicer1e as a non-canonical regulator of cell metabolism

Marta Wojnicka, Arkadiusz Kajdasz, Lukasz Marczak, Piotr H. Malecki, Aleksander Strugala, Klaudia Wojcik, Konrad Kuczynski, Anna Philips, Anna Kurzynska-Kokorniak*

Institute of Bioorganic Chemistry, Polish Academy of Sciences, 61-704 Poznan, Poland

*corresponding author: akurzyns@man.poznan.pl

Abstract

Background

Alternative transcript isoforms contribute to functional diversification of the proteome by generating protein variants with distinct structural and regulatory properties. Dicer1e is a naturally occurring truncated protein isoform of human Dicer (hDicer) detected in both physiological and cancer-associated contexts; however, its biochemical activity and biological function remain poorly understood.

Methods

Dicer1e was ectopically expressed in HEK293T cells and hDicer-deficient HEK293T NoDice cells. Its biochemical properties were characterized using *in vitro* RNA cleavage assays, while its structural features were predicted using AlphaFold3. Cellular effects were evaluated by RNA sequencing, quantitative proteomics, RT-qPCR, immunoblotting, and proliferation assays.

Results

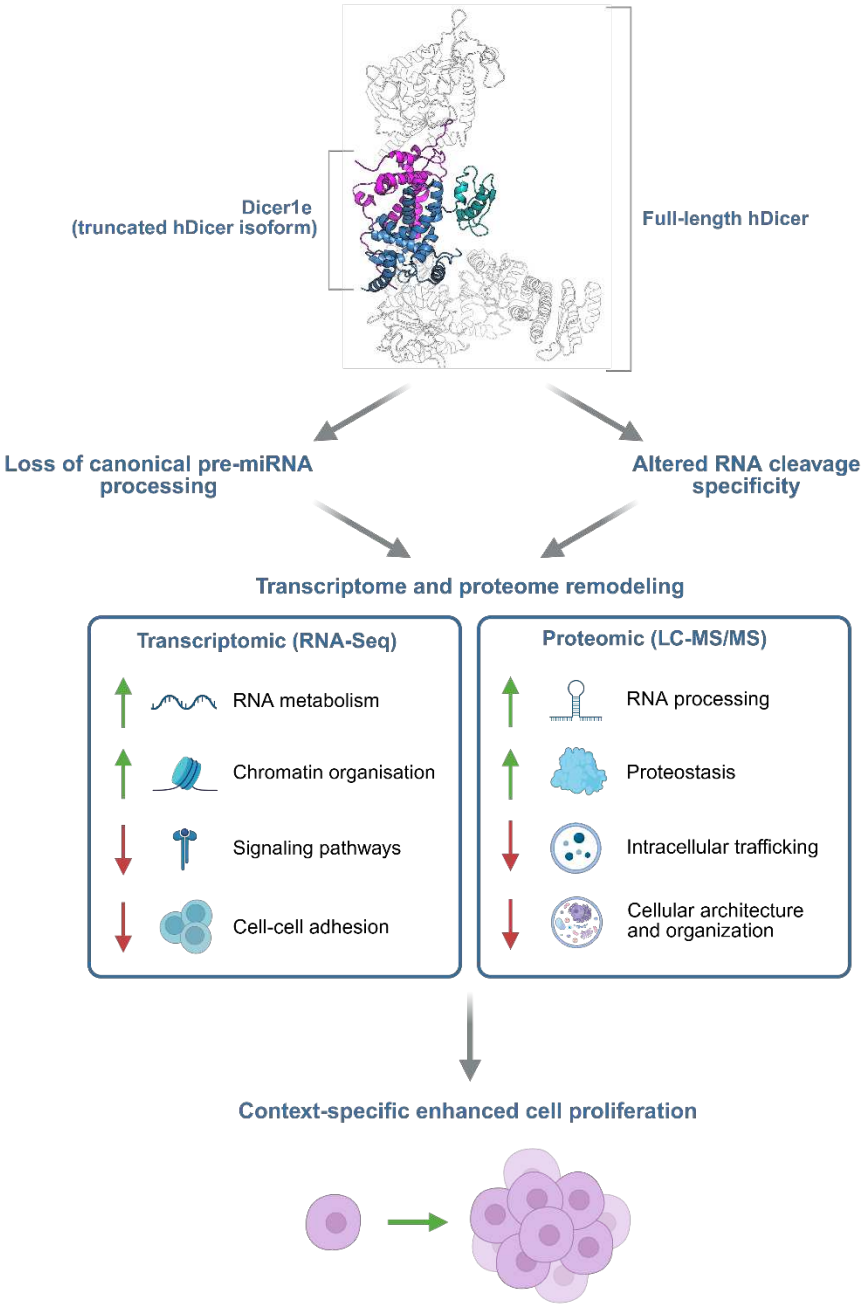
Dicer1e retained Mg^{2+}-dependent RNase activity but did not generate canonical ~21–22-nucleotide hDicer cleavage products, instead producing heterogeneous RNA fragments, consistent with altered substrate positioning following loss of the Platform and PAZ domains. Structural modeling revealed preservation of the catalytic RNase III core together with a unique, evolutionarily conserved 13-amino-acid N-terminal extension, which is predicted to contribute to the distinct structural properties of the isoform. Dicer1e expression induced extensive, context-dependent remodeling of cellular regulatory networks. Although transcriptomic and proteomic datasets exhibited limited overlap at the level of individual genes and proteins, both analyses converged at the biological pathway level, highlighting alterations in RNA metabolism, intracellular organization, vesicle-mediated transport, cellular signaling, and proliferation. These molecular responses differed substantially between HEK293T and

HEK293T NoDice cells, indicating that endogenous hDicer modulated the cellular consequences of Dicer1e expression. Consistent with these observations, Dicer1e promoted proliferation more prominently in hDicer-deficient cells than in cells expressing endogenous hDicer.

Conclusions

These findings identify Dicer1e as a specialized RNase with biochemical and regulatory properties distinct from those of full-length hDicer. More broadly, this study demonstrates that alternative transcript isoforms can generate functionally specialized protein variants with biological properties distinct from those of their canonical counterparts, highlighting the importance of considering alternative *DICER1* transcripts as potential contributors to RNA regulation.

Keywords: Dicer1e, human Dicer, transcript isoforms, RNase III, RNA cleavage, miRNA, transcriptomics, proteomics, cell proliferation.



53

54 **Graphical abstract**

55 Figure generated in BioRender software.

Introduction

The functional complexity of eukaryotic gene expression is substantially expanded by alternative transcript usage, which enables the generation of multiple RNA and protein isoforms from a single gene. Differential isoform expression contributes to the diversification of cellular regulatory mechanisms during development, differentiation, and adaptation to stress, while dysregulated isoform expression is frequently associated with pathological states, including cancer [1, 2]. In such contexts, alternative transcript usage can generate protein variants with altered localization, interaction networks, enzymatic properties, or regulatory functions. These observations suggest that alternative protein isoforms may provide additional layers of cellular regulation beyond the functions of their canonical counterparts.

The human Dicer1e isoform represents a particularly intriguing truncated variant of human Dicer (hDicer) detected in both physiological and cancer-associated conditions, with elevated expression linked to highly proliferative cellular states [3, 4]. These observations suggest that Dicer1e may fulfill specialized regulatory functions distinct from those of canonical full-length hDicer.

Dicer proteins belong to the ribonuclease III (RNase III) family of endoribonucleases that catalyze site-specific cleavage of phosphodiester bonds within double-stranded RNAs (dsRNAs) in a divalent cation-dependent manner, typically involving Mg^{2+} ions [5]. In mammals, Dicer is predominantly localized in the cytoplasm, where it plays a central role in microRNA (miRNA) biogenesis. Dicer recognizes hairpin-shaped precursor miRNAs (pre-miRNAs) of ~50–70 nucleotides (nt) in length and processes them into miRNA duplexes containing the functional mature miRNAs. These miRNAs, through the RNA-induced silencing complex (RISC), guide sequence-specific gene regulation by binding to complementary sites in target messenger RNAs (mRNAs), leading to translational repression or mRNA degradation [6-8].

The human *DICER1* gene gives rise to multiple transcript variants, including several isoforms encoding the canonical full-length hDicer protein [3, 4, 9-11]. These isoforms differ mainly in their 5′ and 3′ untranslated regions, while the coding sequence remains unchanged. The 1,922-residue (~220 kilodaltons, kDa) hDicer protein comprises an N-terminal helicase domain, DUF283 (domain of unknown function), Platform, PAZ, Connector helix, two RNase III domains (RNase IIIa and IIIb), and a dsRNA-binding domain (dsRBD) [12-15] (Figure 1A). The RNase III domains dimerize to form a dsRNA-cleavage valley; each domain cleaves one RNA strand, and together they generate products with 5′-phosphate, 3′-hydroxyl ends and two-base 3′ overhangs [5, 16, 17]. A structural region comprising the Platform, PAZ, and Connector helix, termed the PPC cassette, is critical for pre-miRNA recognition [18, 19]. It contains a 3′-overhang-binding pocket within the PAZ domain and two distinct 5′-end-binding pockets, with specificity toward different substrate termini, spanning the Platform and PAZ domains [19, 20]. The distance between these pockets and the RNase IIIa/IIIb catalytic centers determines the length of miRNAs (~21–22 nt) produced by hDicer [21, 22].

Endogenously expressed hDicer isoforms lacking one or more canonical domains have attracted increasing attention, as accumulating evidence from other mammalian systems suggests that such truncated variants may perform distinct and biologically relevant functions [23-25]. Like its mammalian orthologs, hDicer preferentially processes pre-miRNA rather than precursor small interfering RNA (pre-siRNA) substrates. This substrate selectivity is partially mediated by the N-terminal helicase domain, which acts as a regulatory gatekeeper by restricting the productive binding of long dsRNAs [25-28]. Deletion of the helicase domain markedly enhances hDicer's efficiency in processing pre-siRNAs [29]. Truncated hDicer variants lacking portions of the helicase domain can arise via alternative splicing and have been detected in human embryonic stem cells, induced pluripotent stem cells, and certain human cell

lines [30]. In these contexts, they have been shown to exhibit altered substrate specificity and to contribute to antiviral defense by enabling efficient processing of viral dsRNA.

In addition to physiologically relevant contexts, truncated forms of hDicer have also been observed under pathological conditions. One such example is the t-Dicer variant detected in neuroblastoma cells, which arises from aberrant splicing and lacks part of the RNase IIIb domain and the C-terminal dsRBD domain [9]. Functional analyses demonstrated that t-Dicer exhibits impaired pre-miRNA processing activity compared with full-length hDicer, highlighting the importance of hDicer domain architecture for canonical RNA cleavage [31].

Additional truncated hDicer isoforms, including the Dicer d (~113 kDa) and Dicer e (~93 kDa) variants, have been identified in breast cancer cells, further underscoring the functional relevance of hDicer domain architecture in oncogenic contexts [4]. These isoforms differ markedly in domain composition. The Dicer d isoform retains the Platform, PAZ, and RNase IIIa domains, whereas Dicer e contains both RNase III domains together with the C-terminal dsRBD domain [4] (Figure 1A). Notably, both isoforms were detected in breast cancer cells exhibiting an epithelial phenotype but were absent following epithelial-to-mesenchymal transition and in cells with a mesenchymal phenotype associated with increased motility, invasiveness, and metastatic potential [4].

The Dicer e variant, also known as Dicer1e, arises from alternative splicing of the *DICER1* primary transcript [3]. Translation of Dicer1e initiates at exon 22, and alternative splicing leads to skipping of the 5′ portion of exon 23, resulting in a frameshift. Consequently, the N-terminal region of the protein is altered: the first 13 amino acids differ from those of full-length hDicer, and the region corresponding to amino acids 14–1115 is absent (Figure 1B). Beyond breast cancer, Dicer1e has also been detected in oral cancer cell lines representing both epithelial and mesenchymal phenotypes, where it predominantly localizes to the nucleus [3]. Although Dicer1e has been detected in normal control cells, its expression levels are significantly elevated

in cancer cells [3]. Silencing of Dicer1e resulted in a pronounced reduction in cancer cell proliferation and was associated with induction of apoptosis or cell cycle arrest at interphase [3]. Moreover, depletion of Dicer1e sensitized cancer cells to the chemotherapeutic agent cisplatin, although the molecular mechanisms underlying this effect remain unclear [3].

Analysis of publicly available transcriptomic data from the GEPIA2 database [32] has revealed that the DICER1-014 transcript variant (Ensembl ID: ENST00000556045.5), which likely corresponds to the Dicer1e isoform, is highly expressed in healthy testicular tissue (Supplementary Figure S1A). Together with previous observations [3], these findings indicate that Dicer1e is not a cancer-specific isoform but is also expressed under physiological conditions, suggesting a broader biological relevance. However, Dicer1e's biochemical properties and molecular functions remain largely undefined. Notably, Dicer1e retains both RNase III domains and the C-terminal dsRBD domain, while lacking the N-terminal helicase domain as well as the Platform and PAZ domains required for canonical pre-miRNA recognition by full-length hDicer. This domain architecture raises fundamental questions regarding the enzymatic competence of Dicer1e and its potential contribution to RNA-mediated regulatory pathways.

Given this knowledge gap, we investigated the impact of Dicer1e on cellular gene expression programs and proteome composition using transcriptomic and proteomic approaches, followed by functional assessment of its effects on cell proliferation. We further examined whether Dicer1e retains RNase III-dependent nuclease activity and employed structure-based molecular modeling to gain mechanistic insight into its functional potential. Together, our results provide novel insights into the functional potential of Dicer1e and its impact on cellular regulatory networks.

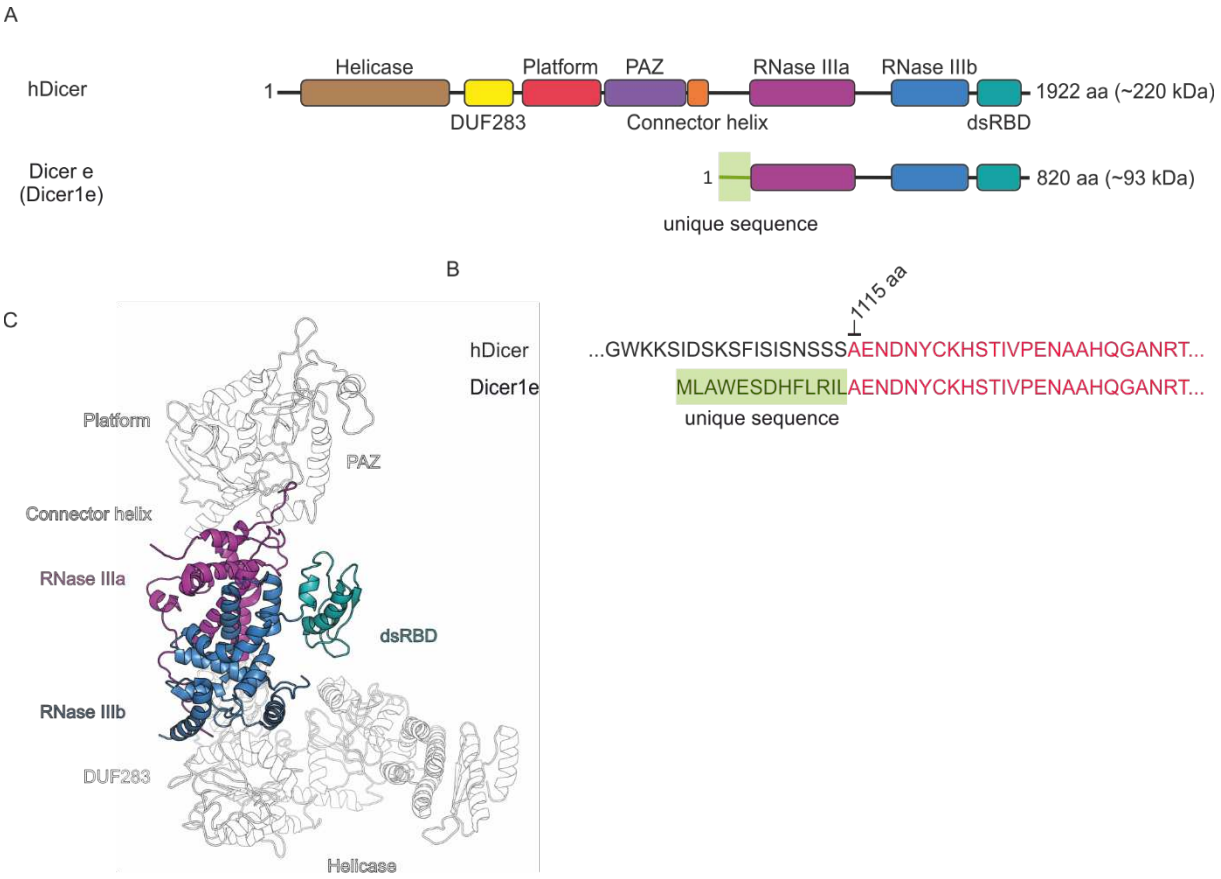


Figure 1

Structural organization of full-length hDicer and the Dicer1e isoform. **(A)** Schematic representation of the domain architecture of hDicer and Dicer1e. The unique 13-amino-acid N-terminal sequence of Dicer1e is highlighted in green. **(B)** Alignment of the N-terminal amino acid sequences of hDicer and Dicer1e. **(C)** Three-dimensional structure of hDicer (PDB: 5ZAL) visualized in PyMOL. Domains retained in Dicer1e are shown in color, whereas domains absent from Dicer1e are depicted as white cartoons outlined in gray.

Materials and Methods

Oligonucleotides

DNA and RNA oligonucleotides (Table 1) were purchased from Genomed (Warsaw, Poland) and FutureSynthesis (Poznan, Poland), respectively.

Table 1. Oligonucleotide sequences

Name	**Sequence 5′ – 3′**
pre-miRNA 16-1	5′ – UAGCAGCACGUAAAUAUUGGCGUUAAGAUUCUAAAAUUAUCUCCAGUAUUAACUGUGCUGCUGAA – 3′
RNA21	5′ – UCGAAGUAUUCCGCGUACGUG – 3′
RNA32	5′ – GUGCAUUGUAGUUGCAUUGCAUGUUCUGGUCA – 3′
RNA32_ov	5′ – ACCAGAACAUGCAAUGCAACUACAAUGCACAU – 3′
OVH_a	5′ – GCCTCGAGATTGATCTACCATGGACTACAAAGACGATGACGACAAGATGCTGGCGTGGGAGTCAGATCACTTCCTGCGGATTTTAGCTGAAA – 3′
OVH_b	5′ – AAGCAATTGTGCTGTGCTTACAGTAATTATCATTTTCAGCTAAAATCCGCAGGAAGTGATCTGACTCCCACGCCAGCATCTTGTCGTCATCGT – 3′
1e_F_qPCR	5′ – CCTGCGGATTTTAGCTGAA – 3′
1e_R_qPCR	5′ – ATCTGCTGAAACTTCAACG – 3′
FL_F_qPCR	5′ – CGGATTTTAGATACCCTAACT – 3′
FL_R_qPCR	5′ – TCACAGACATTTGGTCATG – 3′
fACT_qPCR	5′ – CGACATGGAGAAAATCTGG – 3′
rACT_qPCR	5′ – ATAGCACAGCCTGGATAG – 3′
Fr_mir21	5′ – GCTTATCAGACTGATGTTGAAA – 3′
Fr_mir16-1	5′ – GCACGTAAATATTGGCGAA – 3′
Fr_mir92a	5′ – TTCCACTTGTCCCGGCCTGTAA – 3′
for_ov	5′ – GCCTCGAGATTGATCTACCATG – 3′
rev_ov	5′ – AAGCAATTGTGCTGTGCTTACAG – 3′
SV1e_for	5′ – ATCACTTCCTGCGGATTTTAGCTGAAAATGATAATTACTGTAAG – 3′
SV1e_rev	5′– CTGACTCCCACGCCAGCATGGTGGCCCTCCTCTTAAAGTTTAAAC – 3′
Fw-GFP/C	5′ – ATGGTGAGCAAGGGCGAGG – 3′
Rv-GFP/C	5′ – GGATCCGAGCTCGGTACC – 3′
Fw-GFP-1e/C	5′ – ACCGAGCTCGGATCCATGCTGGCGTGGGAGTCA – 3′
Rv-GFP-1e/C	5′ – GCCCTTGCTCACCATGCTATTGGGAACCTGAGGTTGATT – 3′

Note: the overlapping sequences for OE-PCR are underlined.

Preparation of the Dicer1e and Dicer1e (D1320A/D1709A) expression plasmids

The expression plasmid encoding full-length hDicer fused at the C-terminus with a 3×FLAG epitope (hDicer::3×FLAG) was previously constructed in our laboratory [33]. The hDicer::3×FLAG plasmid served as a template for generating a construct encoding the Dicer1e splice variant. The *Dicer1e* construct was obtained by PCR amplification using Herculase II Fusion DNA Polymerase (Agilent; cat. no. 600675), according to the manufacturer's instructions. The PCR was designed to simultaneously amplify the coding sequence of the Dicer1e variant and the plasmid backbone. Primers used for the amplification (SV1e_for and SV1e_rev; sequences provided in Table 1) included 19-nt overhangs at their 5′ ends corresponding to the unique 39-nt N-terminal sequence of *Dicer1e*, in addition to sequences complementary to the vector and the hDicer sequence. The resulting PCR product, comprising the complete expression plasmid with the Dicer1e coding sequence, was phosphorylated using T4 polynucleotide kinase (Thermo Fisher Scientific; cat. no. EK0032) and ligated with T4 DNA Ligase (Promega; cat. no. M1801), according to the manufacturers' instructions.

To generate a construct encoding the Dicer1e variant with RNase III domain mutations (D1320A/D1709A), the plasmid pCAGGS-FLAG-hsDicer (D1320A/D1709A) (Addgene; plasmid #41585) was used as a backbone [34]. This plasmid contains point mutations in both RNase IIIa (D1320A) and RNase IIIb (D1709A) domains. A 4088-base pair (bp) fragment containing the FLAG Tag (46 bp) and a 4042-bp fragment of the *DICER1* sequence was excised using *XhoI* and *MunI* restriction enzymes. To replace the excised fragment, a 125-bp synthetic DNA sequence encoding the unique N-terminal region of *Dicer1e* fused to a 3×FLAG Tag at the 5′ end was designed and synthesized in two overlapping fragments (OVH_a and OVH_b; sequences listed in Table 1). The two fragments were assembled via overlap extension PCR (OE-PCR) using primers for_ov and rev_ov (Table 1). The assembled product was digested with *XhoI* and *MunI* and ligated into the previously prepared plasmid backbone using T4 DNA

Ligase. All constructs, including *Dicer1e* and *Dicer1e (D1320A/D1709A)*, were verified by Sanger sequencing (Genomed, Warsaw, Poland).

Preparation of the Dicer1e-GFP expression plasmid

The Dicer1e-GFP construct was generated using a restriction enzyme-free cloning approach with the In-Fusion Snap Assembly Master Mix (Takara Bio; cat. no. 638947), according to the manufacturer's instructions. This recombination-based system enables precise assembly of DNA fragments through 15-nt homologous overlaps engineered at the ends of the insert and vector sequences. The pcDNA-GFP plasmid encoding green fluorescent protein (GFP) (Addgene; plasmid #160697) was used as the backbone vector. The coding sequence of *Dicer1e* was PCR-amplified from previously generated FLAG-tagged constructs, as described above, using the primer pairs Fw-GFP-1e/C and Rv-GFP-1e/C (Table 1). The primer pair contained 15-nt overlapping regions compatible with the vector sequence. In parallel, the pcDNA-GFP vector was PCR-linearized to generate ends suitable for recombination. Linearization was performed using the primer pair Fw-GFP/C and Rv-GFP/C (Table 1). The PCR-amplified insert and the linearized vector were combined at a 1:1 molar ratio and subjected to the In-Fusion assembly reaction according to the standard protocol. The resulting construct was transformed into Stellar Chemically Competent Cells (Takara Bio; cat. no. 636763). Positive clones were verified by Sanger sequencing (Genomed, Warsaw, Poland).

Preparation of dsRNA

To prepare dsRNA substrates, non-labeled RNA32_ov was hybridized, at a molar ratio of approximately 1:1, with ^{32}P-labeled complementary RNA32 in a buffer containing 50 mM NaCl, 2.5 mM $MgCl_2$, and 20 mM Tris-HCl (pH 7.5), by heating up to 95°C and then slowly cooling down to room temperature.

The 5′-end oligonucleotide labeling

Oligonucleotides were radiolabeled as previously described [35, 36]. In brief, oligonucleotide (10 µM) was labeled with 1 µL of [γ^{32}P] ATP (3000 Ci/mmol, Hartman Analytic GmbH; cat. no. SRP-401) and 10 U T4 polynucleotide kinase (Thermo Fisher Scientific; cat. no. EK0032) for 10 min at 37°C. The radiolabeled oligonucleotides were PAGE-purified in 8% denaturing polyacrylamide gels and resuspended in water to a final concentration of approximately 10,000 cpm/µL.

hDicer and Dicer1e cleavage assay

Cleavage reactions were carried out in 10 µL volumes using a buffer containing 50 mM NaCl, 2.5 mM $MgCl_2$, and 20 mM Tris-HCl (pH 7.5). Each reaction mixture contained approximately 5 nM of ^{32}P-labeled RNA substrate and 12.5 nM of the recombinant protein. A no-enzyme control was included in each experiment. Where indicated, reactions were supplemented with 25 mM EDTA to assess divalent cation dependence. All reactions were incubated at 37°C for 15, 30, or 60 min in the presence of RNaseOUT™ Recombinant Ribonuclease Inhibitor (Thermo Scientific; cat. no. 10777019). Reactions were terminated by adding an equal volume of 7 M urea loading buffer (prepared by dissolving urea in water at 50°C), followed by heating at 95°C for 5 min. Cleavage products were resolved on 15% denaturing polyacrylamide gels using 1× TBE as the running buffer.

Cell Culture and Transfection

HEK293T and HEK 293T NoDice cells [37] were cultured in DMEM (Gibco, Thermo Fisher Scientific; cat. no. 11965092) supplemented with 10% Fetal Bovine Serum HI (FBS) (EURx; cat. no. E5051-02), Penicillin-Streptomycin (100 U/mL of penicillin and 100 µg/mL of streptomycin) (Gibco, Thermo Fisher Scientific; cat. no. 15140122) and 1 mM Sodium Pyruvate (Gibco, Thermo Fisher Scientific; cat. no. 11360070), as described in Bogerd et al.

[37]. Transfection was carried out by DharmaFECT kb DNA Transfection Reagent (Dharmacon, Abo; cat. no. T-2006-01), according to the manufacturer's instructions. HEK 293T NoDice cell lines were kindly provided by Prof. Bryan R. Cullen [37]. Transfections for RNA-Seq, proteomics, and protein production experiments were performed using 7 µg of plasmid DNA.

Immunoprecipitation

Cells were harvested 48 hours post-transfection by centrifugation at 1,500 rpm for 3 min and suspended in lysis buffer containing 30 mM HEPES (pH 7.4), 100 mM KCl, 5 mM $MgCl_2$, 10% glycerol, 0.5 mM DTT, and 0.2% Tergitol, supplemented with protease inhibitor cocktail (without EDTA; Roche/Merck; cat. no. 4693132001). Cells were lysed by repeated passage through a 0.9 × 40 mm needle. Lysates were cleared by centrifugation at 13,000 rpm for 5 min at 4°C, and the supernatant was incubated overnight at 4°C on a rotator with ANTI-FLAG® M2 Affinity Gel (Merck; cat. no. A2220) pre-washed with TBS buffer (50 mM Tris HCl, 150 mM NaCl, pH 7.4). Following incubation, the resin was washed five times with TBS buffer, and bound proteins were eluted using 100 µg/mL 3×FLAG Peptide (Merck; cat. no. F4799). Eluted proteins were resuspended in storage buffer (20 mM Tris-HCl, pH 7.5; 50 mM NaCl; 10% glycerol; 0.25% Triton X-100). Protein concentrations were determined using the Bradford assay (Bio-Rad; cat. no. 5000006) against a BSA standard curve and verified by SDS-PAGE with BSA standards.

Protein extraction for Western blot analysis

For total protein isolation, cell pellets (~8×10^6 cells) were resuspended in 200 µL of RIPA buffer (50 mM Tris-HCl, pH 7.4; 150 mM NaCl; 1% NP-40; 0.5% sodium deoxycholate; 0.1% SDS; 1 mM DTT), supplemented with cOmplete™ EDTA-free Protease Inhibitor Cocktail (Roche; cat. no. 11873580001). The suspension was incubated on ice for 20 min with periodic

vigorous vortexing. Lysates were clarified by centrifugation at 13,000 rpm for 10 min at 4°C, and the resulting supernatant was collected for Western blot analysis. Cytoplasmic and nuclear protein fractions were prepared from cell pellets (~3×10^6 cells) using the NE-PER® Nuclear and Cytoplasmic Extraction Kit (Thermo Fisher Scientific; cat. no. 78833), following the manufacturer's instructions. Protein concentrations in all lysate fractions were determined using the Pierce™ BCA Protein Assay Kit (Thermo Fisher Scientific; cat. no. 23225) according to the manufacturer's protocol.

Western blot analysis

A total of 20 µg of either whole-cell lysates or subcellular protein fractions was resolved by 8% SDS-PAGE and transferred onto PVDF membranes (Thermo Fisher Scientific, Waltham, MA, USA). Membranes were blocked overnight at 4°C in 3% non-fat dried milk prepared in phosphate-buffered saline containing 0.1% Tween-20 (PBS-T). Following blocking, membranes were incubated overnight at 4°C with one of the following primary antibodies: anti-Dicer (F-10, 1:300; Santa Cruz Biotechnology, sc-136979), anti-β-Actin (D6A8, 1:1100; Cell Signaling Technology), anti-Lamin B1 (nuclear envelope marker, 1:800; Abcam, ab16048), or anti-DYKDDDDK tag (D6W5B, 1:800; Cell Signaling Technology). After incubation, membranes were washed four times with PBS-T and then incubated for 1 h at room temperature with the appropriate horseradish peroxidase (HRP)-conjugated secondary antibody, either anti-mouse or anti-rabbit (1:1000; Jackson ImmunoResearch Laboratories, Inc., Cambridgeshire, UK). Signal detection was performed using SuperSignal™ West Pico PLUS Chemiluminescent Substrate (Thermo Fisher Scientific) according to the manufacturer's instructions, and the Alliance Q9 Advanced imaging system (UVITEC).

Isolation of total RNA and mRNA fractions

Total RNA was extracted using the TRIzol™ Reagent (Invitrogen, Thermo Fisher Scientific; cat. no. 15596026) following the manufacturer's standard protocol. mRNA was isolated using the RNeasy Mini Kit (Qiagen; cat. no. 74104), according to the manufacturer's instructions. To minimize genomic DNA contamination, on-column DNase treatment was performed using the RNase-Free DNase Set (Qiagen; cat. no. 79254) during the RNA purification process. RNA quantity and purity were assessed using a NanoDrop One spectrophotometer (Thermo Fisher Scientific). Isolated RNA fractions were stored at -80°C until further use.

Reverse transcription and quantitative PCR

To generate cDNA for the quantitative analysis of selected miRNAs, 4 μg of total RNA was reverse-transcribed using the Mir-X™ miRNA First Strand Synthesis Kit (Takara Bio; cat. no. 638315), following the manufacturer's instructions. For quantification of *DICER1* expression, 0.8 μg of mRNA was reverse-transcribed using the SuperScript III Reverse Transcriptase (Thermo Fisher Scientific; cat. no. 18080093), according to the manufacturer's protocol. Quantitative PCR (qPCR) was performed using 8 ng of cDNA per reaction with gene- or miRNA-specific primers and the iTaq™ Universal SYBR® Green Supermix (Bio-Rad; cat. no. 1725121). The following primers were used: for miRNA 16-1: Fr_mir16-1; for miRNA 21: Fr_mir21; for miRNA92a: Fr_mir92; for *DICER1*: FL_F_qPCR and FL_R_qPCR; for *Dicer1e:* 1e_F_qPCR and 1e_R_qPCR, for *ACTB*: fACT_qPCR and fACT_qPCR (Table 1). Reactions were run on a CFX96™ Real-Time PCR Detection System (Bio-Rad), and Ct values were determined using the instrument's software. miRNA expression levels were normalized to U6 small nuclear RNA, and mRNA expression levels were normalized to *ACTB* (β-actin) mRNA. The relative levels of selected miRNAs were evaluated by using the $2^{-\Delta\Delta}$Ct method [38], and the relative expression level of genes of interest was evaluated by using the $2^{-\Delta}$Ct method. All experiments were performed in three independent biological replicates, each with three technical replicates. No-template control reactions were included to confirm the absence of

316 contamination. The amplification efficiency of primers for all analyzed miRNAs was assessed
317 and ranged from 90% to 118%, with correlation coefficients (R^2) between 0.988 and 0.998
318 (Supplementary Figure S1C). The obtained data were analyzed by GraphPad Prism 6.0 software
319 (GraphPad Software) using the one-way ANOVA test, with Dunnett's multiple comparisons test
320 or unpaired two-tailed Student's *t*-test.

321 **Cell proliferation assay**

322 HEK293T and HEK293T NoDice cells were seeded in 24-well plates and cultured under the
323 conditions described in the *Cell Culture and Transfection section*. Transfection was performed
324 using FuGENE HD Transfection Reagent (Promega; cat. no. E2311) at a plasmid-to-reagent
325 ratio of 1:3, according to the manufacturer's instructions. Briefly, 1 µg of plasmid encoding
326 hDicer1e-GFP was used per well. Each 24-well plate included the following conditions for both
327 HEK293T and HEK293T NoDice cells: untransfected cells, cells treated with transfection
328 reagent only (mock-transfected cells), and cells transfected with hDicer1e-GFP. To assess cell
329 mortality, the apoptotic dye Incucyte Cytotox Red Dye (Sartorius; cat. no. 4632) was added to
330 all wells according to the manufacturer's protocol. For each condition, 10 technical replicates
331 were analyzed across three independent biological experiments. Green (GFP) and red (Cytotox
332 Red) fluorescence, as well as cell confluence as a measure of viability, were monitored for up
333 to 72 h post-transfection, with images acquired every 2 h. Live-cell imaging and fluorescence
334 measurements were performed using the Incucyte S3 Live-Cell Analysis System with G/R
335 Optical Module (Sartorius) with the use of green (excitation: 441–481 nm; emission: 503–544
336 nm) and red (excitation: 567–607 nm; emission: 622–704 nm) fluorescence channels. All
337 micrographs were taken using a 10X objective lens with a resolution of 1.24 µm/pixel. Data
338 from this experiment were processed in Sartorius Incucyte software version 2022A with the
339 fluorescence correction calibration current on the day of the measurements. Further data

processing, including statistical analysis and graph preparation, was performed using GraphPad Prism 9.0 software (GraphPad Software). Statistical significance was assessed using the Brown–Forsythe and Welch ANOVA followed by Dunnett's T3 multiple comparisons test. For cell proliferation analysis, control cell lines were compared exclusively with GFP-positive cells.

RNA sequencing (RNA-Seq)

For library preparation and RNA-Seq, total RNA was delivered to European Sequencing Center Ltd. (Warsaw, Poland). Strand-specific RNA-Seq libraries were prepared, and sequencing was performed on the BGI next-generation sequencing platform using the DNBSEQ technique [39] in paired-end mode.

RNA-Seq data analysis

Raw reads were mapped to the human genome (primary assembly version GRCh38, release 104, downloaded from Ensembl) using STAR (v2.7.11a) [40]. Reads mapped to exons were counted with featureCounts (v2.0.6) [41]. Only read pairs with both ends aligned were taken into account. Read pairs in which the two reads were aligned to different chromosomes or to different strands of the same chromosome were excluded. Gene coverage and reads distribution in gene features (exons, introns, CDS, 5′UTRs, 3′UTRs, above gene and below gene) were calculated using the geneBody_coverage.py and read_distribution.py scripts, respectively, both of which are part of RSeQC package (v5.0.3) [42]. In both scripts, the gene models file hg38_GENCODE_V47.bed, provided by RSeQC, was used.

The subsequent steps of the analysis were performed in *R* (v4.4.1). Differentially expressed genes were identified using edgeR (4.2.1) [43]. Comparisons were carried out between: (i) HEK293T cells expressing Dicer1e versus mock-transfected HEK293T controls, and (ii) HEK293T NoDice cells expressing Dicer1e versus mock-transfected NoDice controls. Genes

with at least 10 reads in a minimum 50% of samples were retained for downstream analyses. Heatmaps were generated with the mixOmics package (v6.28.0) [44].

Raw reads are available in the GEO database under the GSE336410 accession number.

Gene Ontology enrichment analysis

Gene ontology (GO) terms for differentially expressed protein-coding genes (false discovery rate FDR < 0.05 and $|\log_2 FC| > 1$) were identified across three GO categories: biological process (BP), cellular component (CC) and molecular function (MF) using the topGO package (v2.56.0). The org.Hs.eg.db (v3.19.1) database was used to identify GO terms. Fisher's exact test was employed to assess GO terms enrichment (Supplementary Tables S6–S9).

Protein extraction for MS analysis

Cell culture pellets were suspended in 200 µL of 50 mM ammonium bicarbonate with 1% Sodium Deoxycholate (Sigma Aldrich; cat. no. D6750-25G). Samples were vortexed for 5 min and subsequently homogenized with PRECELLYS24 (BERTIN Instruments®) operated at 5,000 rpm, for 3 x 30 s cycles. Samples were then shortly spun and sonicated on ice for 10 min. Homogenized samples were centrifuged for 10 min at 14,000 rpm in 4°C (Hettich UNIVERSAL 320 R). The supernatant was collected into the new vials. The protein concentration of the samples was determined by the BCA assay. For in-solution digestion, an aliquot containing 10 µg of protein was brought to the appropriate volume up to 25 µL of 50 mM ammonium bicarbonate buffer. Disulfide bonds were reduced by incubation with 5.6 mM DTT at 95°C for 5 min. Subsequently, free thiol groups were alkylated using 5 mM iodoacetamide (IAA) for 20 min at room temperature in the absence of light. Proteolytic digestion was initiated by adding 0.2 µg of sequencing-grade trypsin (Promega; cat. no. V5280), followed by overnight incubation at 37°C. The reaction was then quenched with 1.5 µL of 10%

trifluoroacetic acid (TFA), mixed for 10 min, and centrifuged twice at 12,000 rpm for 7 min at 20°C. The resulting tryptic peptides were subsequently subjected to LC–MS/MS analysis.

Proteome analysis

Proteomic analysis was performed using a Dionex UltiMate 3000 RSLC nanoLC system coupled to Exploris 480 Orbitrap mass spectrometer (Thermo Fisher Scientific). Peptides were separated on an Acclaim PepMap RSLC nanoViper C18 reversed-phase analytical column (75 µm × 25 cm, 2 µm particle size) maintained at 30°C, using a flow rate of 300 nL/min. Chromatographic separation was performed using a 190-min linear gradient of acetonitrile from 4 to 60% in 0.1% formic acid.

Mass spectrometric (MS) data were acquired in positive ion mode using a data-dependent acquisition (DDA) Top10 method over an m/z range of 300–2000. Full MS scans were acquired at a resolution of 60,000 at m/z 200, whereas MS/MS spectra were recorded at a resolution of 15,000 at m/z 200. The ten most abundant precursor ions with charge states of 2+ or higher were selected for fragmentation by higher-energy collisional dissociation (HCD) using a normalized collision energy of 28%.

Raw data were processed in Proteome Discoverer 2.2 software (Thermo Fisher Scientific). Protein identification was performed against the UniProt human database, with precursor mass tolerance set to 10 ppm and fragment ion mass tolerance set to 0.08 Da. Carbamidomethylation of cysteine residues was set as a fixed modification, while methionine oxidation was considered as a variable modification. Up to two missed cleavage sites were allowed. Proteins were considered confidently identified when at least two peptides were assigned to a given protein and the FDR was below 1%, as determined using the Percolator algorithm.

For relative quantitative analysis, label-free normalization was performed in Proteome Discoverer 2.2. Statistical analysis was subsequently carried out in Perseus software version

2.0.11.0. Data visualization, including graphical presentation of the results, was prepared using SRPlot.

Functional enrichment and protein-protein interaction network analyses were performed using the STRING database. Lists of differentially abundant proteins were submitted to STRING using *Homo sapiens* as the reference organism. Protein-protein interaction networks were generated based on the STRING interaction database, and functional enrichment analyses were performed for the submitted protein sets. Enrichment results, including GO categories, pathway annotations and other functional terms provided by STRING, were exported as tab-delimited tables. The exported enrichment tables were further processed in R, and graphical visualization was performed using the ggplot2 package. Enrichment plots were generated as dot plots, in which the enrichment score was calculated as $-\log_{10}$ of the FDR, point size reflected the number of annotated background proteins associated with a given term, and point colour represented the number of significant proteins assigned to the term. Different point shapes additionally indicated functional categories.

The mass spectrometry proteomics data have been deposited to the ProteomeXchange Consortium via the PRIDE partner repository with the dataset identifier PXD078975. The dataset includes raw LC-MS/MS files and processed search results supporting the proteomic analyses presented in this study.

Comparison of transcriptomic and proteomic datasets

To assess the relationship between transcript and protein abundance, the analysis was restricted to biomolecules identified in both datasets that met the thresholds for differential expression (FDR < 0.05 for genes; $p < 0.05$ for proteins). Pearson correlation coefficients were calculated based on $\log_2$ fold changes using the ggscatter function from the ggpubr package (v0.6.3) in R (v4.4.1).

Modeling of Dicer1e and its interactions with RNA

Structural modeling of the human Dicer1e isoform was performed using AlphaFold3 via the AlphaFold Server (https://alphafoldserver.com/) [45]. To model the tertiary structure of the Dicer1e variant, the primary amino acid sequence of the truncated variant (UniProt: A0A076VAC5) was utilized, and predictions were executed using default parameters. To investigate the potential single-stranded RNA-binding capacity of Dicer1e, a complex was structurally predicted by providing the Dicer1e protein sequence alongside a 21-nt RNA sequence (5′ – UCGAAGUAUUCCGCGUACGUG – 3′) as separate chain entities. The models are available in ModelArchive (modelarchive.org) with the accession codes ma-hrci9, and ma-1vauu [46].

Model structural confidence was assessed using per-atom predicted local distance difference test (pLDDT) for localized structural flexibility, predicted aligned error (PAE) matrices to judge relative domain orientations, and the predicted template modeling (pTM) score to confirm global topology validity. Structural visualizations were created using PyMOL Molecular Graphics System.

Results

Research model to study the potential biological role of Dicer1e

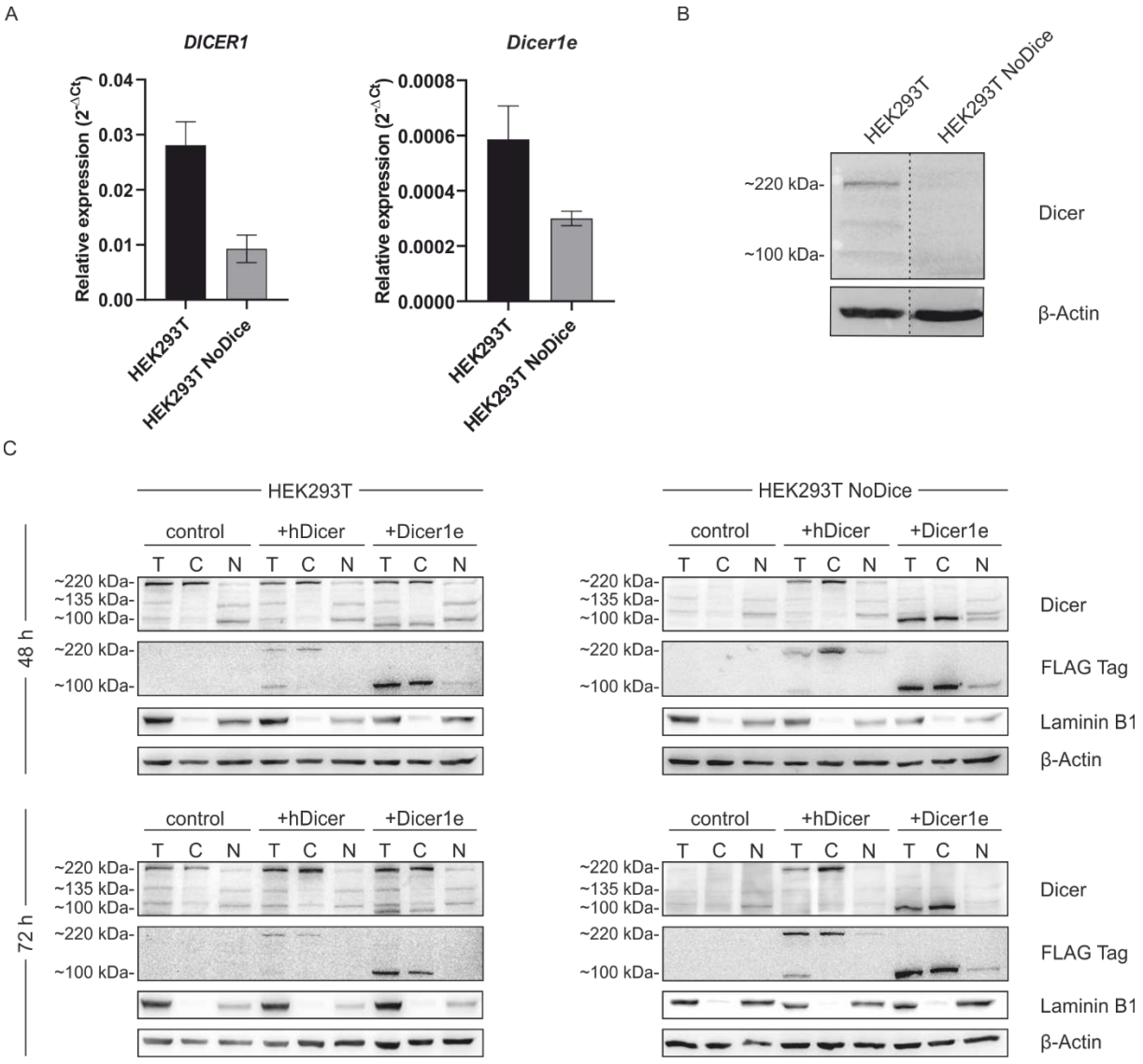
The Dicer1e protein has been detected in both cancer-associated and physiological contexts [3, 4] (Supplementary Figure S1A), suggesting that this isoform is not restricted to malignant cells and may also perform physiological functions. To investigate its potential functional properties outside of cancer-derived cellular models, we expressed Dicer1e in human embryonic kidney HEK293T cells and in the *DICER1* knockout derivative HEK293T NoDice cells [37].

HEK293T NoDice cells transcribe the mutated *DICER1* gene (Figure 2A), but do not produce full-length hDicer protein (Figure 2B) [37]. RT-qPCR analysis with hDicer isoform-specific primers demonstrated that both HEK293T and NoDice cells express Dicer1e mRNA (Figure 2A). Previous studies described Dicer1e as a ~93 kDa protein localized to both the cytoplasm and nucleus [3, 4]. In our experiments, immunoblot analysis of HEK293T and NoDice cells revealed truncated hDicer variants of ~130 and ~100 kDa, predominantly present in nuclear fractions (Figure 2C). However, due to the lack of Dicer1e-specific antibodies, we could not unambiguously assign the ~100 kDa band to the Dicer1e isoform. In HEK293T cells, the full-length hDicer protein (~220 kDa) was primarily detected in the cytoplasmic fraction (Figure 2C).

To assess the expression and localization of recombinant Dicer1e protein, HEK293T and NoDice cells were transiently transfected with an expression vector encoding FLAG-tagged Dicer1e (Figure 2C). In parallel, separate cultures of both cell lines were transfected with a construct expressing a FLAG-tagged full-length hDicer, which served as a control (Figure 2C). Cells were harvested 48 and 72 hours post-transfection for Western blot analysis. In cells transfected with the FLAG-tagged Dicer1e construct (predicted molecular mass of the Dicer1e-3×FLAG protein: 96.3 kDa), recombinant Dicer1e was detected mainly in the cytoplasm,

473 although a minor fraction was also present in the nucleus. Recombinant Dicer1e protein levels
474 remained comparable between 48 and 72 hours post-transfection. FLAG-tagged full-length
475 hDicer was predominantly detected in the cytoplasmic fraction of both HEK293T and NoDice
476 cells, consistent with its expected subcellular localization.

477 Together, these results establish HEK293T and HEK293T NoDice cells as suitable
478 experimental models for investigating Dicer1e function and demonstrate that recombinant
479 Dicer1e is stably expressed predominantly in the cytoplasmic compartment, with a minor
480 fraction detectable in the nucleus.



481

482 **Figure 2**

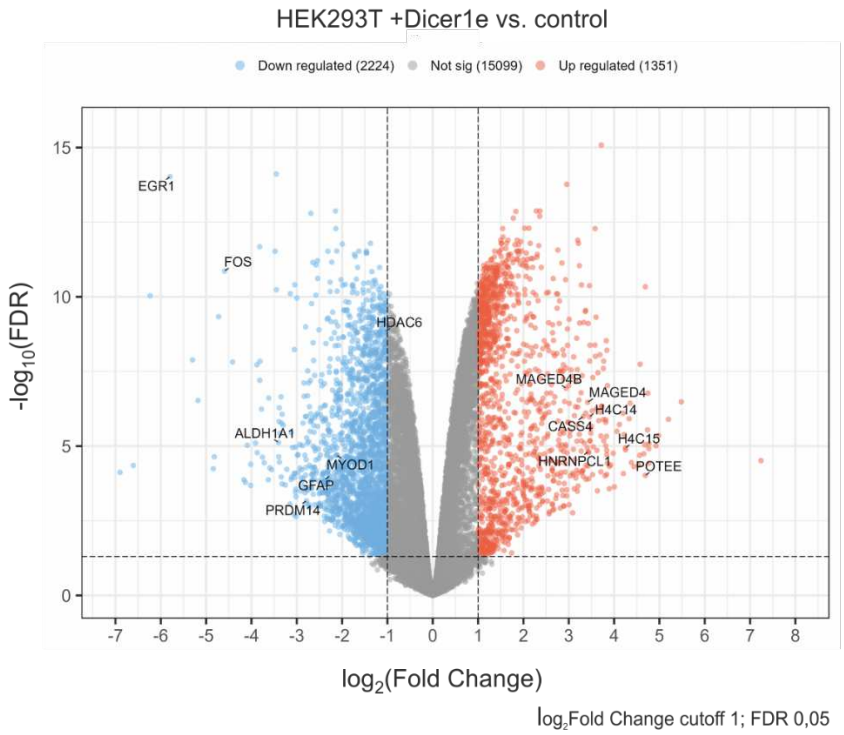
Expression and subcellular localization of hDicer and Dicer1e in HEK293T and HEK293T NoDice cells. (A) Relative expression of *DICER1* and the *Dicer1e* transcript in HEK293T and NoDice cells determined by RT-qPCR. Transcript levels were normalized to *ACTB* expression. Data are presented as mean ± SD from three biological replicates (n = 3). (**B**) Western blot analysis of endogenous hDicer protein in HEK293T and HEK293T NoDice cells. (**C**) Subcellular localization of recombinant FLAG-tagged Dicer1e in HEK293T and NoDice cells. Nuclear (N), cytoplasmic (C), and total (T) protein fractions were isolated 48 and 72 h after transfection with a FLAG-tagged Dicer1e expression vector (+Dicer1e). Cells transfected with FLAG-tagged full-length hDicer (+hDicer) or treated with transfection reagent alone (control) served as controls. Equal amounts of protein (20 μg) were analyzed by Western blot using antibodies against hDicer, FLAG Tag, Laminin B1, and β-Actin. Laminin B1 was used as a nuclear marker, whereas β-Actin served as a loading control.

Comparison of gene expression profiles in HEK293T and HEK293T NoDice cells expressing the Dicer1e variant

To investigate the impact of the Dicer1e isoform on global gene expression, transcriptome profiling was performed in HEK293T and HEK293T NoDice cells following ectopic expression of Dicer1e protein. RNA sequencing (RNA-Seq) was conducted 48 hours after transfection under two experimental conditions in each cell line: mock-transfected controls and Dicer1e-expressing cells, with three biological replicates per condition (12 samples total). An average of 51.7 million paired-end reads (150 bp) was generated per sample. The majority of reads aligned to annotated gene regions in the human reference genome (GRCh38), indicating high library quality and effective alignment (Supplementary Figure S1B and Supplementary Table S1). Differential gene expression analysis was performed to assess transcriptional

changes induced by Dicer1e expression in each cellular background. Genes with low expression were excluded prior to analysis, resulting in 18,848 genes retained in the HEK293T dataset (Supplementary Table S2) and 18,991 genes in the HEK293T NoDice dataset (Supplementary Table S3). In HEK293T cells, Dicer1e expression resulted in significant changes affecting 3,575 genes (FDR < 0.05 and $|\log_2 FC| \geq 1$), including 1,351 upregulated and 2,224 downregulated transcripts, whereas 15,099 genes showed no significant changes in expression (Supplementary Table S4). The overall distribution of differentially expressed genes (DEGs) and clustering heat maps are shown in Figure 3A and Supplementary Figure S2A, respectively. In HEK293T NoDice cells, Dicer1e expression resulted in significant changes in 1,770 genes (FDR < 0.05 and $|\log_2 FC| \geq 1$), of which 759 were upregulated, and 1,011 were downregulated, whereas 17,221 genes showed no significant expression changes (Supplementary Table S5). Corresponding DEG distribution and clustering heat maps are presented in Figure 3B and Supplementary Figure S2B. These results indicate that Dicer1e expression induces broad transcriptional alterations, with a markedly stronger effect in cells expressing endogenous full-length hDicer.

A



B

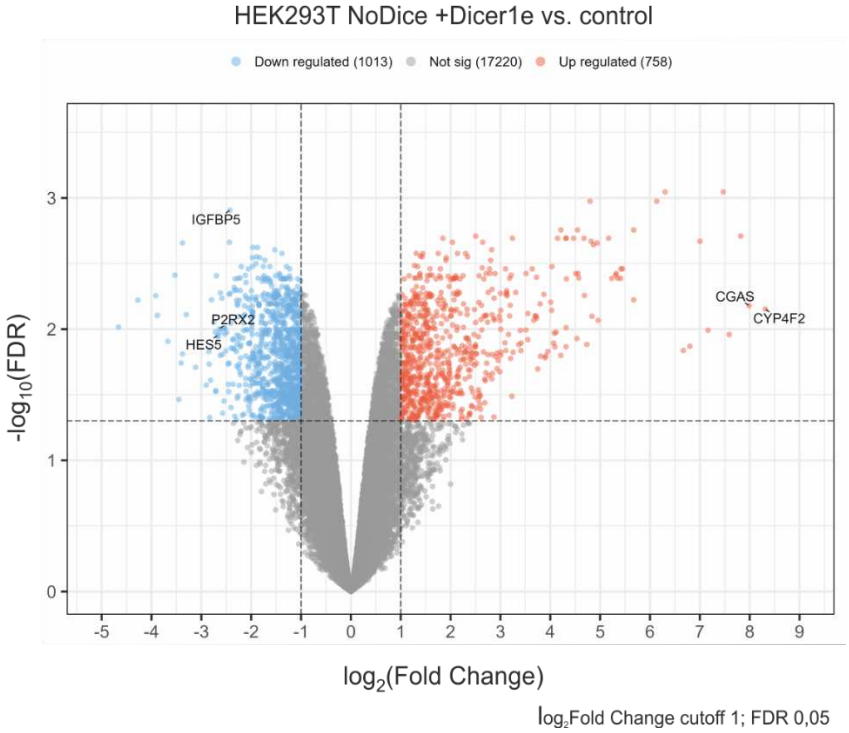


Figure 3

Volcano plots showing differential gene expression following Dicer1e expression. (**A**) HEK293T cells. **(B)** HEK293T NoDice cells. Differentially expressed genes (DEGs) were defined as genes with FDR < 0.05 and $|\log_2 FC| > 1$. The x-axis represents $\log_2$ fold change in

gene expression, and the y-axis represents -$\log_{10}$(FDR). Each dot corresponds to a single gene. Significantly upregulated genes are highlighted in red and downregulated genes in blue, whereas non-significant genes are shown in gray. The data were generated from three independent biological replicates per condition (n = 3). Cancer-associated genes exhibiting the strongest expression changes (FDR < 0.05 and $|\log_2 FC| \geq 2$) are indicated.

To characterize the biological processes affected by Dicer1e expression, Gene Ontology (GO) enrichment analysis was performed on protein-coding DEGs (FDR < 0.05 and $|\log_2 FC| \geq 1$) identified in each cell line. In HEK293T cells, genes upregulated upon Dicer1e expression were predominantly enriched in biological processes related to RNA metabolism and processing, including ribosomal RNA, transfer RNA, messenger RNA, and non-coding RNA processing, as well as ribosome biogenesis (Figure 4A and Supplementary Table S6). Enriched molecular functions were associated with RNA binding and catalytic activity acting on RNA, while cellular component analysis highlighted mitochondrial structures and extracellular organization. Conversely, downregulated genes in HEK293T cells were enriched in biological processes associated with cell adhesion, morphogenesis, differentiation, and cell–cell signaling. These genes were linked to molecular functions related to cytokine activity and receptor binding, and to cellular components localized at the plasma membrane and extracellular regions (Figure 4A and Supplementary Table S7). In HEK293T NoDice cells, genes upregulated upon Dicer1e expression were predominantly enriched in biological processes related to transcriptional regulation and chromatin organization, including regulation of transcription by RNA polymerase II, chromatin remodeling, nucleosome assembly, and DNA recombination (Figure 4B and Supplementary Table S8). Corresponding molecular functions and cellular components were predominantly associated with DNA binding, chromatin structure, and chromosome-associated complexes. Downregulated DEGs in HEK293T NoDice cells were

enriched in biological processes related to cell adhesion, regulation of cell population proliferation, and receptor-mediated signaling pathways, with prominent representation of immune-related categories. These genes were largely associated with receptor activity and plasma membrane localization (Figure 4B and Supplementary Table S9). Together, these findings demonstrate that Dicer1e modulates distinct functional gene networks depending on the presence or absence of full-length hDicer.

Next, to identify transcriptional changes induced by Dicer1e independently of endogenous hDicer, DEGs were compared between HEK293T and HEK293T NoDice cells expressing Dicer1e. These analyses identified 318 commonly regulated protein-coding genes, including 59 upregulated and 259 downregulated genes (Supplementary Table S10). GO enrichment analysis of commonly upregulated genes revealed overrepresentation of processes related to non-coding RNA processing, regulation of transcription by RNA polymerase II, immune system regulation, and protein phosphorylation. These genes were enriched for molecular functions associated with DNA binding and transcriptional regulation and were primarily localized to nuclear compartments (Figure 4C and Supplementary Table S11). Commonly downregulated genes were enriched in biological processes involved in cell-cell communication, adhesion, differentiation, and cellular organization. Associated molecular functions included transmembrane transporter and signaling receptor activities, and enriched cellular components were related to cell projections, junctional complexes, and membrane-associated protein assemblies (Figure 4C and Supplementary Table S12). These shared transcriptional signatures suggest that Dicer1e can regulate specific gene expression programs independently of canonical hDicer-mediated pathways.

Given previous reports of Dicer1e expression in cancer tissues [3, 4], we analyzed whether Dicer1e expression affects genes associated with cancer-related processes. To focus on robust

changes, a subset of DEGs exhibiting at least a four-fold change in both cell lines was selected (FDR < 0.05 and $|\log_2 FC| \geq 2$). In both HEK293T and HEK293T NoDice cells, Dicer1e expression altered the transcription of multiple genes involved in cell proliferation, chromatin organization, and immune signaling pathways (Figure 3 and Table 2). Although the specific gene sets differed between the two cellular contexts, these results indicate that Dicer1e modulates cancer-associated pathways in a context-dependent manner.

In summary, Dicer1e expression induces broad transcriptomic alterations in HEK293T and HEK293T NoDice cells and consistently affects a subset of genes independently of endogenous hDicer. Notably, Dicer1e-modulated gene sets are enriched in pathways related to cell proliferation, chromatin organization, and immune signaling – processes that are frequently dysregulated in cancer. These findings suggest a functional role for Dicer1e beyond canonical hDicer activity.

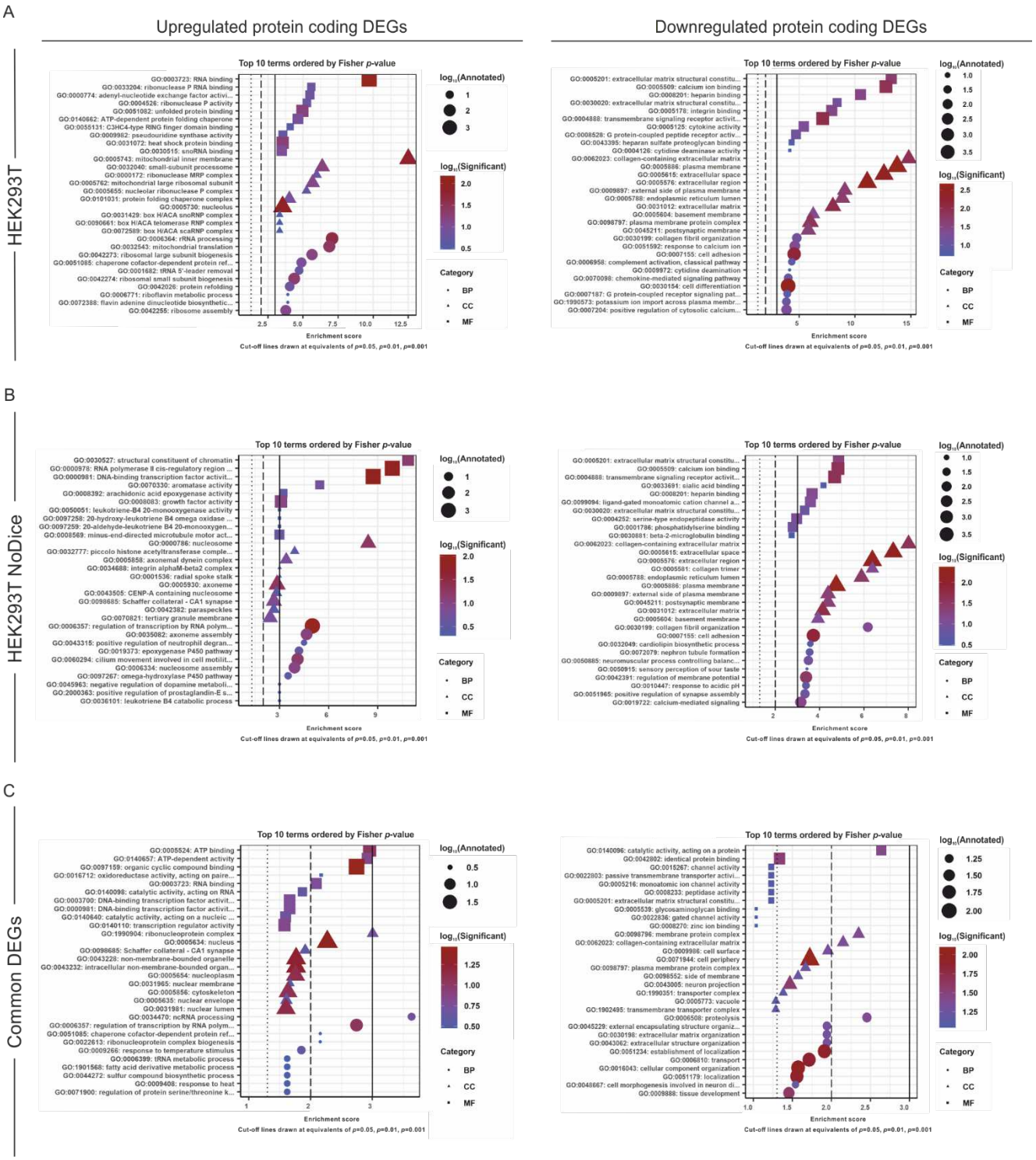


Figure 4

Gene Ontology enrichment analysis of differentially expressed protein-coding genes following Dicer1e expression. **(A)** and **(B)** Enriched GO terms identified among upregulated (left) and downregulated (right) differentially expressed genes (DEGs) in HEK293T and HEK293T NoDice cells, respectively. **(C)** GO enrichment analysis of DEGs shared between

both cell lines. The top 10 enriched terms for the Biological Process (BP), Molecular Function (MF), and Cellular Component (CC) categories are shown, ranked by Fisher's exact test *p*-value.

Proteomic profiling of HEK293T and HEK293T NoDice cells expressing the Dicer1e variant

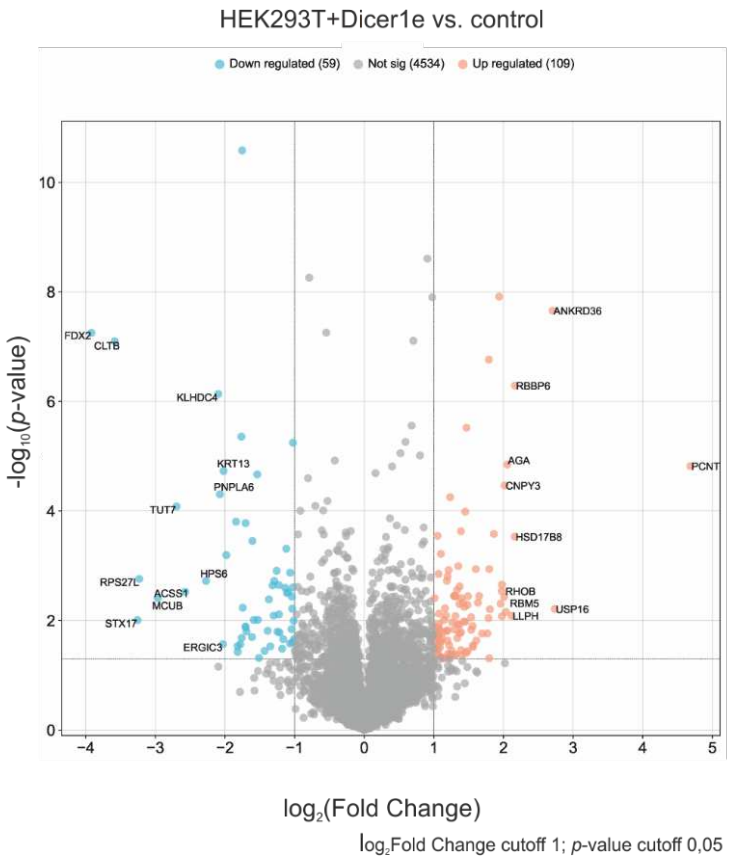
To complement transcriptomic analyses, we performed proteomic profiling of HEK293T and HEK293T NoDice cells following ectopic Dicer1e expression. Analyses were conducted 48 hours post-transfection, matching the RNA-Seq time point, and included at least eight biological replicates per condition. In total, 5,871 proteins were identified across all samples (Supplementary Table S13-S14). Differential protein abundance analysis and subsequent GO enrichment analysis (Supplementary Figure S3) were performed to characterize proteome-wide changes associated with Dicer1e expression in each cellular background. In HEK293T cells, Dicer1e expression resulted in 168 differentially abundant proteins (DAPs) ($p < 0.05$ and $|\log_2 FC| \geq 1$), including 109 upregulated and 59 downregulated proteins (Figure 5A and Supplementary Table S15). In HEK293T NoDice cells, a total of 132 DAPs were identified, of which 46 were upregulated and 86 were downregulated ($p < 0.05$ and $|\log_2 FC| \geq 1$) (Figure 5B and Supplementary Table S16).

To gain insight into the functional consequences of these changes, we focused on a subset of DAPs showing robust and statistically significant alterations in abundance ($p < 0.05$ and $|\log_2 FC| \geq 2$) in both HEK293T and HEK293T NoDice cells expressing Dicer1e. In HEK293T cells, upregulated proteins included PCNT, USP16, ANKRD36A, RBBP6, HSD17B8, LLPH, AGA, RBM5, CNPY3, and RHOB (Figure 5A). These proteins are associated with centrosome organization (PCNT), ubiquitin-dependent protein regulation (USP16, RBBP6), RNA

processing and splicing (RBM5), signal transduction and cytoskeletal dynamics (RHOB), and metabolic or lysosomal pathways (HSD17B8, AGA). Additional proteins, including ANKRD36A, LLPH, and CNPY3, are implicated in protein-protein interactions and cellular homeostasis. Conversely, downregulated proteins included FDX2, CLTB, STX17, RPS27L, MCUB, TUT7, ACSS1, HPS6, KLHDC4, PNPLA6, ERGIC3, and KRT13 (Figure 5A). These proteins participate in mitochondrial function and metabolism (FDX2, MCUB, ACSS1), vesicle-mediated transport and membrane dynamics (CLTB, STX17, ERGIC3, HPS6), RNA metabolism (TUT7), ribosome-associated processes (RPS27L), lipid metabolism (PNPLA6), cytoskeletal organization (KRT13), and protein interaction networks (KLHDC4).

In HEK293T NoDice cells, upregulated proteins included RPUSD3, DICER1, RBM5, and DLG3 (Figure 5B). Notably, the elevated level of DICER1 reflects ectopic expression of the Dicer1e construct introduced by plasmid transfection rather than endogenous protein production. The remaining upregulated proteins are associated with mitochondrial RNA modification (RPUSD3), RNA processing and splicing (RBM5), and membrane-associated scaffolding and signaling (DLG3), indicating modulation of post-transcriptional regulatory pathways and cellular organization. Downregulated proteins included CIR1, PIP4K2A, COG7, SLC4A2, ESPL1, C17orf75, POM121, NIBAN2, and GOLGA4 (Figure 5B). These proteins are associated with transcriptional regulation (CIR1), phosphoinositide signaling (PIP4K2A), Golgi organization and vesicle-mediated transport (COG7, GOLGA4), membrane transport (SLC4A2), cell-cycle progression (ESPL1), nuclear envelope organization (POM121), and cellular stress responses or homeostasis (NIBAN2).

A


HEK293T+Dicer1e vs. control
Down regulated (59)
Not sig (4534)
Up regulated (109)
-log10(p-value)
log2(Fold Change)
log2Fold Change cutoff 1; p-value cutoff 0,05
FDX2
CLTB
KLHDC4
KRT13
PNPLA6
TUT7
HPS6
RPS27L
ACSS1
MCUB
STX17
ERGIC3
ANKRD36
RBBP6
AGA
CNPY3
HSD17B8
RHOB
RBM5
LLPH
USP16
PCNT

B

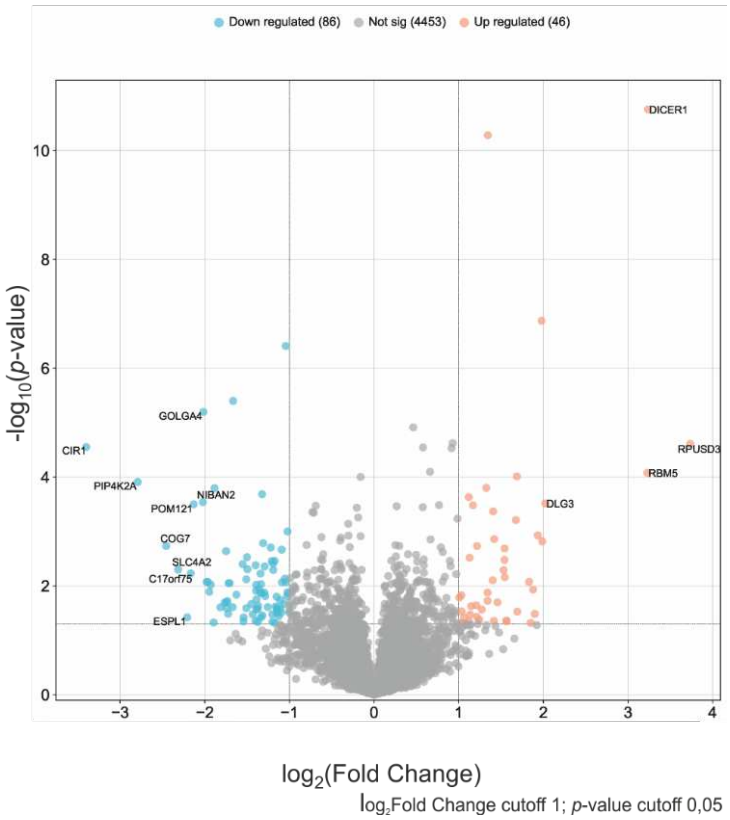

HEK293T NoDice+Dicer1e vs. control
Down regulated (86)
Not sig (4453)
Up regulated (46)
-log10(p-value)
log2(Fold Change)
log2Fold Change cutoff 1; p-value cutoff 0,05
GOLGA4
CIR1
PIP4K2A
NIBAN2
POM121
COG7
SLC4A2
C17orf75
ESPL1
DICER1
RPUSD3
RBM5
DLG3

Figure 5

Volcano plots showing differential protein abundance following Dicer1e expression. (A) HEK293T cells. **(B)** HEK293T NoDice cells. Differentially abundant proteins (DAPs) were defined as proteins with $p < 0.05$ and $|\log_2 FC| \geq 1$. The x-axis represents $\log_2$ fold change in protein abundance, and the y-axis represents $-\log_{10}(p\text{-value})$. Each dot corresponds to a single protein. Significantly upregulated proteins are highlighted in red and downregulated proteins in blue, whereas non-significant proteins are shown in gray. The data were generated from at least 8 independent biological replicates per condition ($n \geq 8$). Selected DAPs exhibiting the strongest abundance changes ($p < 0.05$ and $|\log_2 FC| \geq 2$) are indicated.

Overall, these findings indicate that ectopic Dicer1e expression in HEK293T cells predominantly affected proteins involved in RNA processing, proteostasis, mitochondrial function, and vesicle-mediated transport, whereas in HEK293T NoDice cells, the altered protein abundance profile was more strongly associated with transcriptional regulation, intracellular trafficking, and organelle organization.

Comparison of the two proteomic datasets revealed highly distinct protein abundance profiles in HEK293T and HEK293T NoDice cells, with RBM5 representing the only commonly upregulated protein meeting the applied significance criteria ($p < 0.05$ and $|\log_2 FC| \geq 2$). Despite the limited overlap in individual DAPs between the two cell lines, both proteomic profiles converged at the biological pathway level, indicating that Dicer1e expression consistently affects processes related to RNA metabolism, intracellular organization, and cellular homeostasis, albeit through distinct sets of proteins. Notably, several DAPs identified across the two cellular backgrounds, including RBM5, RBBP6, RHOB, ESPL1, CIR1, and PIP4K2A, have previously been implicated in cancer-associated cellular processes involving regulation of cell proliferation, apoptosis, cytoskeletal organization, transcriptional control, and intracellular

signaling [47, 48], indicating that Dicer1e expression alters the abundance of multiple proteins with established roles in tumor-associated pathways.

To investigate the relationship between transcriptomic and proteomic changes induced by ectopic Dicer1e expression, we compared the corresponding RNA-Seq (Supplementary Tables S2-S3) and proteomic (Supplementary Tables S13-S14) datasets obtained from HEK293T and HEK293T NoDice cells. This analysis revealed only limited overlap between differentially expressed genes and differentially abundant proteins, with no significant correlation between mRNA and protein fold changes, indicating that Dicer1e influences cellular regulation at multiple levels, including post-transcriptional mechanisms.

Collectively, these findings demonstrate that Dicer1e expression induces extensive, context-dependent remodeling of cellular regulatory networks at both the transcriptomic and proteomic levels. Although individual transcriptomic and proteomic alterations showed limited overlap, both datasets converged at the biological pathway level, highlighting RNA metabolism, intracellular organization, vesicle-mediated transport, cellular signaling, and proliferation as major processes affected by Dicer1e expression.

Dicer1e expression is associated with increased proliferative capacity

Given previous reports indicating that Dicer1e is expressed in highly proliferative cellular contexts, including cancer cells [3, 4] and testicular tissue (Supplementary Figure S1A), we next examined whether ectopic Dicer1e expression affects cellular proliferative capacity. Proliferation assays were performed over a 72-hour period following transfection in HEK293T and HEK293T NoDice cells, with three biological replicates analyzed for each condition. In HEK293T cells, ectopic Dicer1e expression led to a moderate increase in cell proliferation compared with control cells, whereas the effect was substantially more pronounced in HEK293T NoDice cells (Figure 6).

These findings indicate that Dicer1e modulates proliferative capacity in a cell context-dependent manner, promoting proliferation more prominently in hDicer-deficient cells than in cells expressing endogenous full-length hDicer. Together with the transcriptomic and proteomic alterations observed upon Dicer1e expression, these results suggest that an altered balance between full-length hDicer and Dicer1e may contribute to cellular processes relevant to tumor biology.

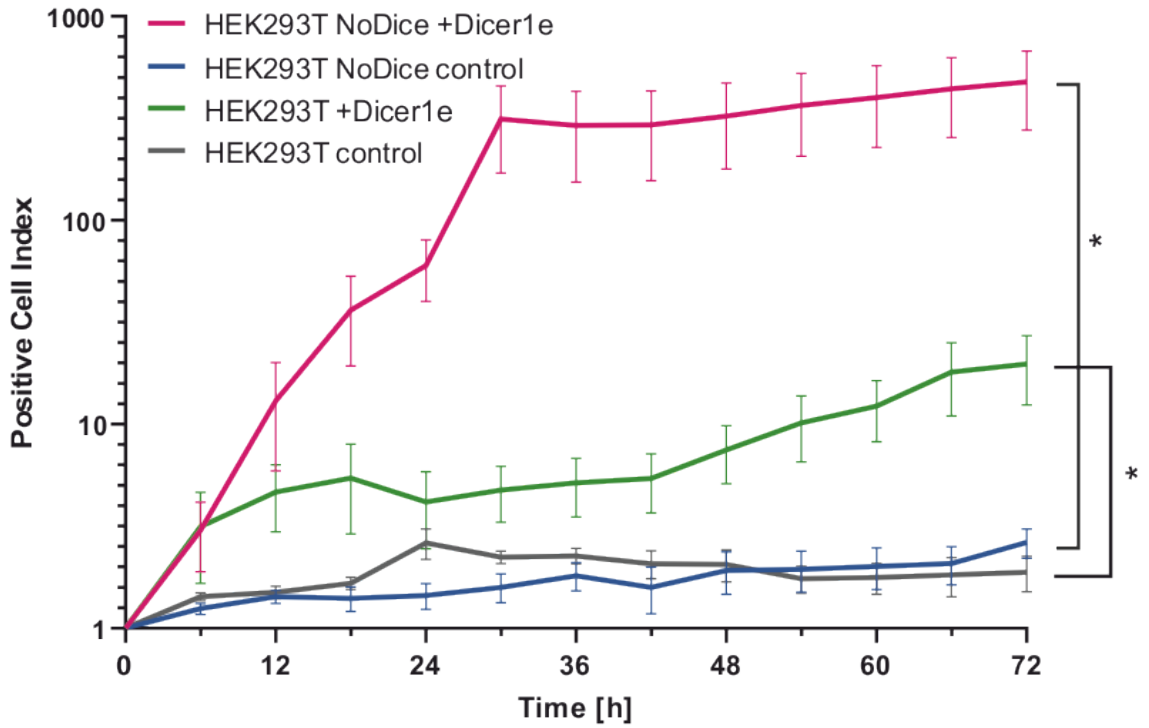


Figure 6

Effects of Dicer1e expression on cell proliferation. HEK293T and HEK293T NoDice cells were transfected with an hDicer1e-GFP expression plasmid or treated with transfection reagent alone (control). Cell growth was monitored for 72 h using the Incucyte S3 Live-Cell Analysis System. Proliferation analyses were restricted to GFP-positive cells to account for transfection efficiency. The positive cell index was normalized to the 0 h time point corresponding to transfection. Data are presented as mean ± SD from three independent biological experiments

(n = 3) with 10 technical replicates per condition. Statistical significance was assessed using the Brown–Forsythe and Welch ANOVA followed by Dunnett's T3 multiple comparisons test. Significance levels are indicated as follows: *p = 0,0294 for HEK293T cells and *p = 0,0278 for HEK293T NoDice cells.

RNA cleavage activity of Dicer1e

The Dicer1e variant retains intact RNase IIIa and RNase IIIb domains as well as the dsRBD domain (Figure 1A). To directly assess the RNase activity of Dicer1e, *in vitro* RNA cleavage assays were performed using recombinant Dicer1e protein. A catalytically inactive Dicer1e variant carrying point mutations in both RNase III domains (D1320A/D1709A) was included as a negative control, as these substitutions have previously been shown to abolish RNase activity of hDicer [34]. Recombinant wild-type hDicer was used as a positive control (Supplementary Figure S4). All recombinant proteins were produced in HEK293T NoDice cells, and RNA cleavage assays were performed using radiolabeled RNA substrates under Mg^{2+}-dependent conditions. Substrate integrity was monitored using reactions lacking protein, with or without EDTA, and cleavage reactions were analyzed over time by denaturing PAGE.

Canonical Dicer substrates were first tested, including pre-miRNA-16-1 and a 30-bp RNA duplex with 2-nt 3′ overhangs (dsRNA_ov) (Supplementary Figure S4B-C). Dicer1e generated multiple cleavage products from pre-miRNA-16-1, which were strongly reduced in the presence of EDTA, indicating Mg^{2+}-dependent RNase activity. No cleavage products were observed with the catalytically inactive Dicer1e mutant, whereas wild-type hDicer produced the expected 21-nt miR-16-1-5p fragment. For the dsRNA_ov substrate, Dicer1e produced a distinct ~8-nt fragment, accompanied by several longer and shorter RNA species that were generated with low efficiency; all of these products were absent in reactions containing the catalytically

inactive mutant or EDTA. Wild-type hDicer generated the characteristic 21-nt product together with ~12-nt and ~11-nt fragments, consistent with previously reported processing patterns (Supplementary Figure S4C) [33]. Overall, Dicer1e did not produce canonical hDicer cleavage products from either substrate.

Our previous studies demonstrated that hDicer associates with RNAs of miRNA length [49] and is capable of hydrolyzing such substrates [33]. Therefore, we next examined whether Dicer1e can also process single-stranded miRNA-sized RNAs using a 21-nt miRNA mimic (ssRNA21) (Supplementary Figure S4D). In the presence of Dicer1e, substrate levels decreased over time, accompanied by accumulation of a ~1–2-nt product. Wild-type hDicer generated similar short products, albeit less efficiently. These products were consistent with previously reported hDicer activity [33]. No cleavage products were detected with the catalytically inactive Dicer1e mutant or under EDTA conditions, confirming the requirement for catalytically active RNase domains and divalent metal ions.

Together, these results demonstrate that Dicer1e retains Mg^{2+}-dependent RNase activity despite lacking the ability to generate canonical hDicer cleavage products. Instead, Dicer1e exhibits altered RNA processing properties, producing heterogeneous cleavage products from both canonical hDicer substrates and miRNA-sized RNAs.

Effects of Dicer1e on cellular miRNAs and miRNA-like species

To investigate whether Dicer1e affects endogenous miRNAs, we analyzed HEK293T and HEK293T NoDice cells transiently expressing Dicer1e. HEK293T NoDice cells lack endogenous hDicer (Figure 2B) and are therefore incapable of canonical pre-miRNA processing. Nevertheless, they retain a heterogeneous population of 16–26 nt small RNAs containing miRNA-derived sequences (hereafter referred to as “miRNA-like species”) [37]. Cells were transfected with plasmids encoding Dicer1e or wild-type hDicer, with mock-

transfected cells as controls. Total RNA was harvested 48 and 72 hours post-transfection, and selected miRNAs (miR-16-1, miR-21, and miR-92a) were quantified by RT-qPCR (Figure 7). These miRNAs were chosen based on their high basal expression in HEK293T cells. Cells transfected with the catalytically inactive Dicer1e mutant (D1320A/D1709A) served as an additional control (Supplementary Figure S4E).

In HEK293T cells, expression of Dicer1e or wild-type hDicer did not significantly alter miRNA levels at either time point (Figure 7A), consistent with the presence of endogenous hDicer. By contrast, HEK293T NoDice cells expressing catalytically active Dicer1e exhibited a marked reduction in all three miRNA-like species at 48 hours (Figure 7B). No decrease was observed with the catalytically inactive mutant (Supplementary Figure S4E). Notably, miRNA-like RNA levels returned to baseline by 72 hours despite persistent Dicer1e expression (Figure 2C and 7B). As expected, expression of wild-type hDicer in HEK293T NoDice cells restored canonical miRNA production, with miR-21 showing the strongest induction at 48 hours and all tested miRNAs substantially elevated by 72 hours (Figure 7B).

Together, these findings indicate that Dicer1e can modulate the abundance of selected miRNA-like species in the absence of endogenous hDicer.

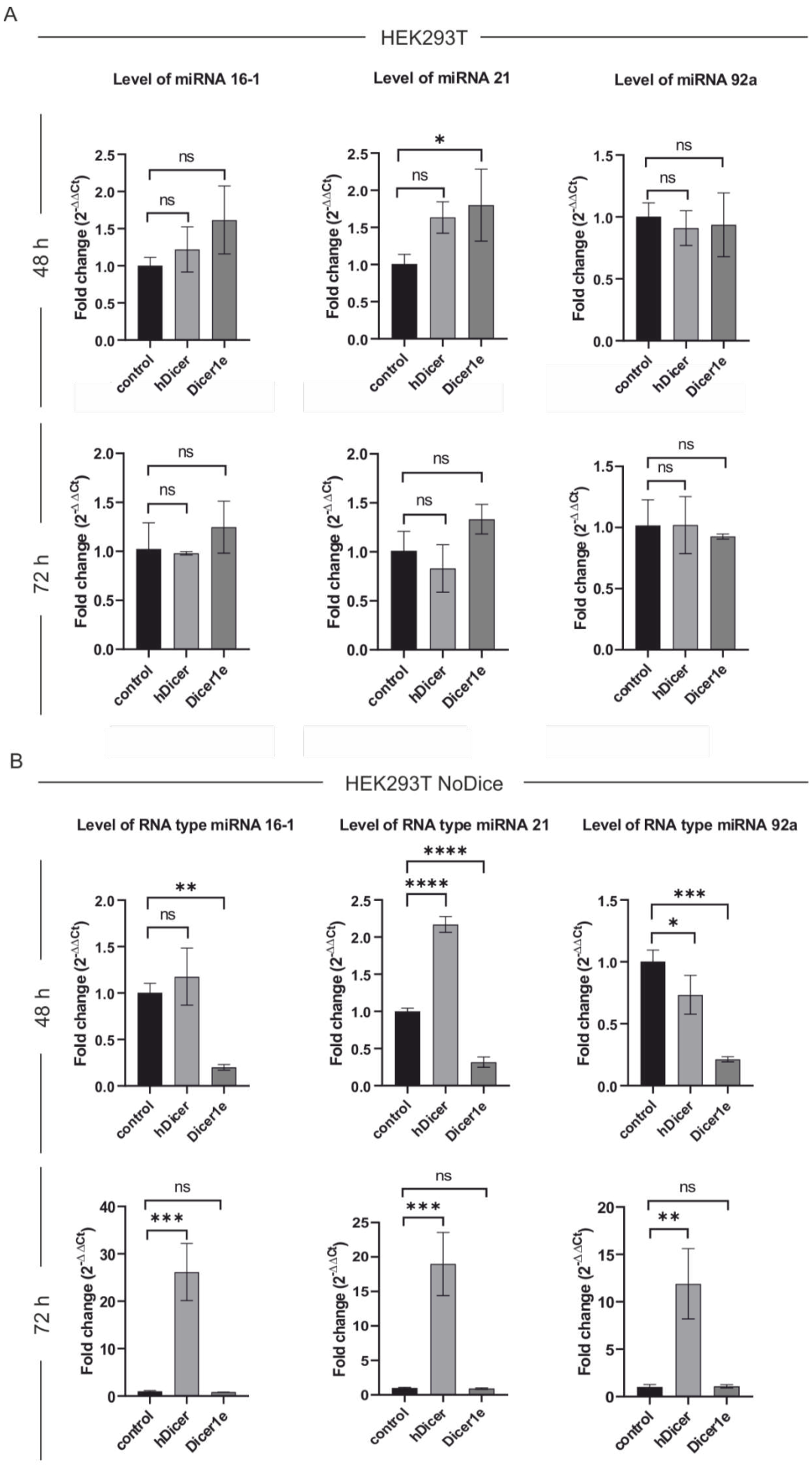

A
HEK293T
Level of miRNA 16-1
Level of miRNA 21
Level of miRNA 92a
48 h
72 h
Fold change ($2^{-\Delta\Delta Ct}$)
control
hDicer
Dicer1e
ns
*
B
HEK293T NoDice
Level of RNA type miRNA 16-1
Level of RNA type miRNA 21
Level of RNA type miRNA 92a
**
***
****

Figure 7

Effects of Dicer1e expression on selected miRNAs and miRNA-like species. Fold changes in the expression of selected miRNAs in HEK293T cells **(A)** and miRNA-like species in HEK293T NoDice cells **(B)** 48 and 72 h after transfection with FLAG-tagged Dicer1e or FLAG-tagged hDicer expression vectors. miRNA/miRNA-like species levels were normalized to U6 snRNA and expressed relative to cells treated with transfection reagent alone (control). Data are presented as mean ± SD from three biological replicates (n = 3). Statistical significance was assessed by one-way ANOVA followed by Dunnett's multiple comparisons test. Significance levels are indicated as follows: *$p < 0.0332$, **$p < 0.0021$, ***$p < 0.0002$, ****$p < 0.0001$.

Structural modeling of Dicer1e reveals a distinct N-terminal architecture and a conserved RNase domain arrangement

To assess the structural consequences of domain truncation in the Dicer1e isoform, we generated a three-dimensional structural model using AlphaFold3 (Figure 8). The region comprising the RNase IIIa, RNase IIIb, and dsRBD domains was predicted with high confidence (Supplementary Figure S5). The overall architecture closely resembled the cryo-EM structure of full-length hDicer (PDB: 5ZAL) [50], supporting the reliability of the predicted fold. In agreement with experimental data [50], several surface-exposed loops within the catalytic core were modeled with low per-residue confidence scores (Supplementary Figure S5 and Supplementary Table S17). These regions correspond to areas that are unresolved in cryo-EM reconstructions of hDicer [50-55], suggesting that they represent intrinsically disordered or highly flexible regions.

A notable structural feature of Dicer1e is its unique N-terminal extension, which is absent in canonical hDicer (Figure 1A-B). In the predicted model, this region adopts a predominantly α-helical conformation positioned within a cleft formed between the two RNase III domains (Figure 8A). Although its placement is spatially defined, the relatively low per-residue confidence scores (Supplementary Figure S5A) indicate that this segment may exhibit conformational flexibility, potentially enabling regulatory or context-dependent structural rearrangements.

To further evaluate the RNA-binding capacity of Dicer1e, we modeled Dicer1e in complex with a 21-nt single-stranded RNA substrate (ssRNA21) (Figure 8B). Structural predictions were generated with AlphaFold3, and the resulting models were ranked according to the algorithm's internal confidence metrics. The top-ranked Dicer1e-RNA complex exhibited a predicted Template Modeling (pTM) score of 0.53, indicating moderate confidence in the overall topology of the protein-RNA assembly and supporting its plausibility as a structural hypothesis. Inspection of the predicted active site revealed that the key catalytic residues within the RNase III domains are positioned in proximity to the RNA substrate but are not oriented to form direct hydrogen bonds. This configuration is consistent with the established catalytic mechanism of Dicer proteins, which require divalent metal ions, preferentially Mg^{2+}, as essential cofactors [5]. Because such ions are not modeled by AlphaFold3, the observed separation between the active site residues and the RNA phosphate backbone is an expected limitation of the prediction rather than an indication of impaired catalytic competence. Nevertheless, the preserved spatial arrangement of the RNase III domains together with the retained accessibility of the catalytic valley is compatible with the experimentally observed RNase activity of Dicer1e (Supplementary Figure S4B–D).

Next, to investigate the evolutionary conservation of the unique N-terminal extension of Dicer1e, we performed a BLASTp search against the GenBank non-redundant protein database using the 13-residue peptide sequence MLAWESDHFLRIL as a query. The analysis revealed strong conservation of this sequence among mammalian Dicer homologs. The highest-scoring hit corresponded to a Dicer isoform from the Sumatran orangutan (*Pongo abelii*) and showed full query coverage. High sequence conservation was also observed across multiple mammalian species, including bats (Figure 8C). These findings indicate that this 13-amino-acid peptide is evolutionarily conserved within the mammalian Dicer lineage, suggesting a potentially important structural or regulatory role in the functional properties of Dicer1e.

Collectively, these analyses indicate that Dicer1e retains the conserved structural organization of the hDicer catalytic core while possessing a unique N-terminal extension that is evolutionarily conserved among mammals.

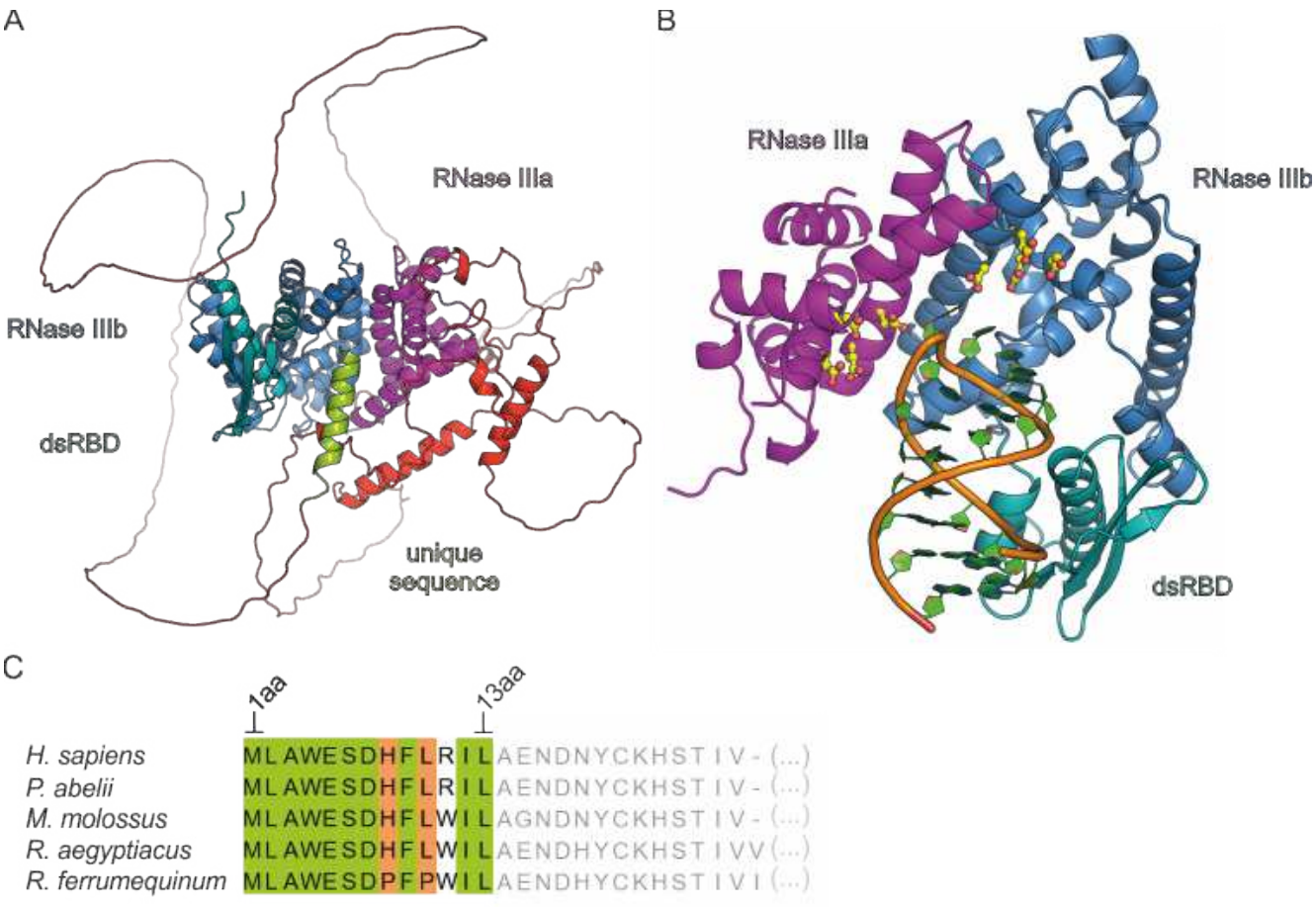


Figure 8

Structural features of Dicer1e revealed by AlphaFold3 modeling and evolutionary analysis. (A) AlphaFold3 model of Dicer1e. The model highlights the conserved catalytic core comprising the RNase IIIa (purple) and RNase IIIb (blue) domains together with the C-terminal dsRBD (teal). The unique 13-amino-acid N-terminal extension is predicted to adopt an α-helical conformation (red/green) and to occupy a position within the shallow cleft between the two RNase III domains. **(B)** AlphaFold3 model of the Dicer1e catalytic core in complex with a 21-nt RNA substrate (orange backbone, green bases). Catalytic residues forming the RNase III active sites are shown as yellow and red balls, and sticks. **(C)** Multiple sequence alignment of amino acids 1–13 comprising the unique N-terminal extension of Dicer1e from *Homo sapiens* (human), *Pongo abelii* (Sumatran orangutan), *Molossus molossus* (Pallas's mastiff bat), *Rousettus aegyptiacus* (Egyptian fruit bat), and *Rhinolophus ferrumequinum* (greater horseshoe bat). Conserved residues are highlighted, demonstrating strong evolutionary conservation within mammals. Truncated downstream sequence boundaries are indicated by parentheses.

Discussion

hDicer ribonuclease is a central regulator of RNA metabolism whose canonical role in miRNA biogenesis is essential for development, differentiation, and cellular homeostasis [11]. Beyond miRNA processing, hDicer also participates in several non-canonical regulatory pathways, including chromatin regulation [56-60], maintenance of genome stability [61-69], and nuclear RNA-associated functions [70]. The broad functional repertoire of full-length hDicer raises the possibility that structural alterations in domain composition may influence its regulatory properties and substrate interactions. In this study, we characterize the human Dicer1e isoform and demonstrate that it represents a catalytically active truncated variant associated with

changes in gene expression, proteome composition, and cell proliferation that are partially independent of full-length hDicer activity.

Dicer1e preserves intact RNase IIIa, RNase IIIb, and dsRBD domains, and *in vitro* assays clearly demonstrate its Mg^{2+}-dependent cleavage activity (Supplementary Figure S4B-C). However, unlike full-length hDicer, Dicer1e does not generate ~21–22 nt products from canonical substrates. Instead, it produces a spectrum of RNA fragments with variable lengths. These products are abolished by catalytic mutations (D1320A/D1709A) or EDTA, confirming that they arise from bona fide RNase-dependent cleavage. The observed heterogeneity of Dicer1e-derived products can be mechanistically explained by the structural consequences of the loss of the Platform and PAZ domains. In full-length hDicer, these domains anchor the pre-miRNA and dsRNA substrate ends, thereby establishing a defined spatial distance between the RNA terminus and the RNase III catalytic centers [21, 22, 71]. In contrast, Dicer1e cannot precisely grip and position the RNA ends. Consequently, substrate engagement is likely mediated predominantly through the dsRBD domain, which may stabilize duplex RNA but does not impose strict distance constraints between the substrate terminus and the RNase IIIa/IIIb catalytic sites [5], potentially resulting in substrate-dependent variability in cleavage site selection and product length.

Our prior experiments indicated that hDicer associates with RNAs of miRNA length [49] and can hydrolyze such substrates [33]. These observations suggested that, beyond its well-established role in miRNA biogenesis, hDicer may also participate in the metabolism of miRNAs that are no longer required by the cell. The present *in vitro* study shows that Dicer1e is also capable of hydrolyzing miRNA-sized RNAs (Figure 7B and Supplementary Figure S4D). Importantly, in HEK293T NoDice cells lacking endogenous hDicer, expression of catalytically active Dicer1e transiently reduced the level of selected miRNA-like species (miR-

16-1, miR-21, and miR-92a) (Figure 7B), whereas the inactive mutant did not (Supplementary Figure S4E). The transient depletion of miRNA-like species in HEK293T NoDice cells suggests that Dicer1e can access and cleave endogenous small RNAs independently of the canonical hDicer pathway. Such activity may influence RNA stability and small RNA turnover. The absence of similar effects in HEK293T cells expressing Dicer1e likely reflects competition or functional dominance by endogenous full-length hDicer. A comparable assessment of the impact of Dicer1e on miRNA expression in HEK293T cells was previously reported by Sawh and Duchaine [72]. In that study, ectopic expression of Dicer1e did not affect miR-19b levels and caused only a modest reduction in the mature-to-precursor ratio of let-7, indicating that the presence of this truncated isoform does not broadly perturb steady-state miRNA abundance in a cellular background containing endogenous full-length hDicer. Structurally, Dicer1e resembles the truncated sDCR-1 variant described in *Caenorhabditis elegans* [72], as both proteins retain the tandem RNase III domains and the C-terminal dsRBD while lacking multiple N-terminal regulatory domains. In the same study, sDCR-1 was shown to arise through proteolytic cleavage of full-length Dicer and to function as a competitive inhibitor of Argonaute proteins, leading to accumulation of pre-miRNAs and a concomitant reduction in mature miRNA levels. Although a similar inhibitory effect on miRNA maturation was not observed for HEK293T cells expressing Dicer1e, the structural similarity between these truncated variants suggests that alternative Dicer forms may represent a conserved strategy for modulating small RNA pathways under specific cellular conditions.

A striking structural feature of Dicer1e is the unique 13-residue N-terminal extension (MLAWESDHFLRIL). BLASTp analysis revealed strong conservation of this 13-residue peptide among mammalian Dicer homologs, including complete identity with the corresponding region in *Pongo abelii* Dicer (Figure 8C). Such strict conservation within mammals argues against this sequence representing a stochastic truncation artifact and instead

supports the notion that it is maintained under selective pressure. The preservation of this short motif suggests that it fulfills a specific structural or regulatory role. Structurally, the peptide is predicted to adopt an α-helical conformation and is positioned between the RNase III domains (Figure 8A), placing it in a strategic location to influence catalytic architecture. One possibility is that it functions as an intramolecular regulatory element, modulating catalytic efficiency or substrate preference through subtle conformational gating of the RNase IIIa/IIIb dimer interface. Given that Dicer1e lacks the PAZ and Platform domains and therefore operates without strict end-anchored measurement, even minor structural constraints imposed by this conserved 13-residue motif could bias substrate alignment within the catalytic valley. Alternatively, the N-terminal fragment may serve as a protein-protein interaction interface, recruiting regulatory cofactors that redirect Dicer1e toward specialized RNA substrates or distinct subcellular compartments. In this context, it could contribute to functional diversification relative to full-length hDicer by enabling isoform-specific interaction networks. Collectively, the evolutionary conservation, predicted structural features, and strategic positioning of this N-terminal segment support its functional relevance and suggest that it contributes to the specialized biochemical and cellular properties of Dicer1e.

Sequence analysis of Dicer1e revealed a putative nuclear localization signal (NLS) between amino acids 247 and 263 [3], while the retained C-terminal dsRBD domain may further facilitate nuclear accumulation of this isoform [73]. In our system, ectopic Dicer1e expression predominantly resulted in cytoplasmic localization, with a minor nuclear fraction consistently detected (Figure 2C). By contrast, pronounced nuclear enrichment of Dicer1e has previously been reported in certain cancer cell types [3], suggesting that its subcellular distribution may be dynamically regulated in a cell-type-dependent manner. Such regulation could influence the accessibility of nuclear RNA substrates and thereby expand the functional repertoire of Dicer1e.

Given that nuclear translocation of full-length hDicer is regulated by phosphorylation [61, 74, 75], similar post-translational mechanisms may also contribute to Dicer1e localization.

In this study, we also demonstrate that Dicer1e exerts broad and context-dependent effects on cellular regulatory networks at both the transcriptomic and proteomic levels. Although the specific sets of differentially expressed genes and differentially abundant proteins differed substantially between HEK293T and HEK293T NoDice cells, both transcriptomic and proteomic analyses converged at the biological pathway level. The predominant alterations involved processes related to RNA metabolism, intracellular organization, vesicle-mediated transport, cellular signaling, and proliferation, indicating that Dicer1e consistently influences core regulatory pathways despite engaging distinct molecular components in different cellular contexts.

Interestingly, only limited concordance was observed between transcriptomic and proteomic datasets. Such discrepancies are commonly reported in multi-omics studies and reflect the combined effects of post-transcriptional regulation, differences in protein turnover, and translational control. In the case of Dicer1e, this observation is particularly intriguing because the protein itself may function as an RNA-processing endonuclease. It is therefore conceivable that Dicer1e modulates cellular regulatory networks through mechanisms extending beyond transcriptional regulation, potentially involving non-canonical RNA substrates or additional post-transcriptional regulatory pathways.

Importantly, several Dicer1e-dependent transcriptomic and proteomic alterations affected pathways associated with cell proliferation, chromatin organization, immune signaling, and intracellular signaling — processes frequently dysregulated in cancer. Consistent with these observations, Dicer1e expression also influenced cellular proliferative capacity. Whereas only a modest increase in proliferation was observed in HEK293T cells expressing endogenous full-

length hDicer, Dicer1e markedly enhanced proliferation in hDicer-deficient HEK293T NoDice cells (Figure 6). These findings suggest that endogenous hDicer modulates the cellular consequences of Dicer1e expression and further support the context-dependent nature of Dicer1e activity.

Conclusions

Our findings demonstrate that Dicer1e is not merely a truncated form of hDicer but rather a functionally distinct RNase with unique biochemical and regulatory properties. Although Dicer1e retains an intact catalytic core and RNase activity, the loss of the Platform and PAZ domains fundamentally alters its substrate processing characteristics, resulting in non-canonical RNA cleavage and context-dependent effects on cellular transcriptomes, proteomes, and proliferative capacity. Together, these observations establish Dicer1e as a catalytically active and functionally distinct hDicer isoform that may regulate cellular processes through mechanisms distinct from those of full-length hDicer.

More broadly, this study shows that alternative transcript isoforms can generate functionally specialized protein variants with biological properties distinct from those of their canonical counterparts. The identification of Dicer1e as a specialized hDicer isoform highlights the importance of considering alternative *DICER1* transcripts as potential contributors to RNA regulation and provides a framework for future studies addressing the physiological and pathological functions of Dicer1e, particularly in highly proliferative tissues and cancer.

968 Table 2. Dicer1e-dependent changes in the expression of cancer-associated genes

Cell line	Regulation after Dicer1e expression	Gene(s)	Reported association with cancer	References
HEK293T	Upregulated	*POTEE, MAGED4, MAGED4B, CASS4, HNRNPCL1*	Genes implicated in tumorigenesis	[76-85]
	Upregulated	*H2B, H4* histone family	Overexpression reported in gliomas, breast cancer, T-PLL, thyroid carcinoma	[86-90]
	Downregulated	*HDAC6*	Reduced expression associated with decreased patient survival	[91]
	Downregulated	*EGR1, FOS, MYOD1, ALDH1A1, PRDM14, GFAP*	Reduced expression linked to increased proliferation and tumor progression	[92-103]
HEK293T NoDice	Upregulated	*CYP4F2*	Context-dependent roles: promotes proliferation in ER+ breast cancer, suppresses growth in HCC	[104, 105]
	Upregulated	*cGAS*	Context-dependent antitumor and protumorigenic effects via cGAS–STING	[106-108]

HEK293T NoDice	Downregulated	*IGFBP5*	Reduced expression associated with enhanced proliferation and tumor growth	[109, 110]
	Downregulated	*HES5*	Involved in proliferation and differentiation in multiple cancers	[111-113]
	Downregulated	*P2RX2*	Reduced expression correlates with poor survival in prostate cancer	[114]

969

Abbreviations

ACTB: beta actin, β-Actin

AH: alkaline hydrolysis

BCA: bicinchoninic acid assay

bp: base pair(s)

DAP: differentially abundant proteins

DDA: data-dependent acquisition

DEGs: differentially expressed genes

dsRBD: double-stranded RNA-binding domain

dsRNA: double-stranded RNA

dsRNA: double-stranded RNA

dsRNA_ov: 30-bp RNA duplex with 2-nt 3′ overhangs

DUF283: Domain of Unknown Function 283

EDTA: ethylenediaminetetraacetic acid

FDR: false discovery rate

GFP: green fluorescent protein

GO: Gene Ontology

HCD: higher-energy collisional dissociation

hDicer: human Dicer

IAA: iodoacetamide

kDa: kilodalton(s)

LC-MS/MS: liquid chromatography–tandem mass spectrometry

miRNA: microRNA

mRNA: messenger RNA

MS: mass spectrometry

nt: nucleotide(s)

OE-PCR: overlap extension polymerase chain reaction

PAE: predicted aligned error

PAGE: polyacrylamide gel electrophoresis

PAZ: Piwi/Argonaute/Zwille domain

pLDDT: predicted local distance difference test

pre-miRNA: precursor microRNA

pre-siRNA: precursor small interfering RNA

pTM: predicted template modeling score

qPCR: quantitative polymerase chain reaction

RISC: RNA-induced silencing complex

RNase III: Ribonuclease III

RNA-Seq: RNA sequencing

rpm: revolutions per minute

RT-qPCR: reverse transcription quantitative polymerase chain reaction

ssRNA21: 21-nt single stranded RNA

TFA: trifluoroacetic acid

Declarations

Acknowledgements

We would like to thank Prof. Bryan R. Cullen for generously providing hDicer-deficient (NoDice) HEK293T human cell lines, Agnieszka Szczepanska for assistance with the preparation and coordination of the RNA-Seq experiments, and all members of the Department of Ribonucleoprotein Biochemistry for their critical reading of the manuscript and valuable comments.

Author contributions

Marta Wojnicka: Conceptualization, Formal analysis, Investigation, Methodology, Visualization, Writing – original draft;

Arkadiusz Kajdasz (transcriptomic analysis): Data curation, Formal analysis, Investigation, Methodology, Visualization;

Lukasz Marczak (proteomic analysis): Data curation, Formal analysis, Investigation, Methodology, Visualization;

Piotr H. Malecki (sequence and structural analysis): Data curation, Formal analysis, Investigation, Methodology, Visualization;

Aleksander Strugala (proteomic analysis): Formal analysis, Investigation;

Klaudia Wojcik (cell proliferation assays): Formal analysis, Investigation, Methodology, Visualization;

Konrad Kuczynski (cell proliferation assays): Formal analysis, Investigation, Methodology, Visualization;

Anna Philips (transcriptomic analysis): Formal analysis, Resources;

Anna Kurzynska-Kokorniak: Conceptualization, Formal analysis, Funding acquisition, Project administration, Resources, Supervision, Writing – original draft, Writing – review & editing.

Consent for publication

All authors have given their consent for the publication of this manuscript. As the study did not involve human participants, individual consent for publication was not required.

Ethics approval and consent to participate

Not applicable.

Competing interests

The authors declare no conflict of interest.

Funding

This research was funded by the National Science Centre, Poland (NCN, grant OPUS 2021/41/B/NZ2/03781 awarded to A.K.K., which supported analyses of Dicer1e subcellular localization and cell proliferation), and also in part by the National Science Centre, Poland (NCN, grant SONATA BIS 2016/22/E/NZ1/00422 awarded to A.K.K., which supported RNase activity assays, transcriptomic analyses, and quantitative proteomics).

Funding for open access charge was provided by the National Science Centre, Poland (NCN, grant OPUS 2021/41/B/NZ2/03781).

For the purpose of Open Access, the authors have applied a CC-BY public copyright license to any Author Accepted Manuscript (AAM) version arising from this submission.

Availability of data and materials

All data generated or analyzed during this study are included in this published article, its supplementary information files, and publicly available repositories.

RNA-Seq data have been deposited in the NCBI Gene Expression Omnibus (GEO) under accession number GSE336410. Proteomics data have been deposited to the ProteomeXchange Consortium via the PRIDE partner repository under dataset identifier PXD078975. Structural models have been deposited in the ModelArchive repository under accession codes ma-hrci9 (Human Dicer1e isoform) and ma-1vauu (Human Dicer1e isoform modeled in complex with a 21-nt RNA substrate). Cell proliferation assay data are available from the corresponding author upon reasonable request.

Further information and requests for resources/reagents should be directed to the corresponding author: Anna Kurzynska-Kokorniak (akurzyns@man.poznan.pl).

References

1. Baralle FE, Giudice J. Alternative splicing as a regulator of development and tissue identity. Nat Rev Mol Cell Biol. 2017;18(7):437-51. doi: 10.1038/nrm.2017.27.
2. Bradley RK, Anczukow O. RNA splicing dysregulation and the hallmarks of cancer. Nat Rev Cancer. 2023;23(3):135-55. doi: 10.1038/s41568-022-00541-7.
3. Cantini LP, Andino LM, Attaway CC, Butler B, Dumitriu A, Blackshaw A, et al. Identification and characterization of Dicer1e, a Dicer1 protein variant, in oral cancer cells. Mol Cancer. 2014;13:190. doi: 10.1186/1476-4598-13-190.
4. Hinkal GW, Grelier G, Puisieux A, Moyret-Lalle C. Complexity in the regulation of Dicer expression: Dicer variant proteins are differentially expressed in epithelial and mesenchymal breast cancer cells and decreased during EMT. Br J Cancer. 2011;104(2):387-8. doi: 6606022 [pii]

10.1038/sj.bjc.6606022.
5. Nicholson AW. Ribonuclease III mechanisms of double-stranded RNA cleavage. Wiley Interdiscip Rev RNA. 2014;5(1):31-48. doi: 10.1002/wrna.1195.
6. Song JJ, Liu J, Tolia NH, Schneiderman J, Smith SK, Martienssen RA, et al. The crystal structure of the Argonaute2 PAZ domain reveals an RNA binding motif in RNAi effector complexes. Nat Struct Biol. 2003;10(12):1026-32. doi: 10.1038/nsb1016

nsb1016 [pii].
7. Meister G, Landthaler M, Patkaniowska A, Dorsett Y, Teng G, Tuschl T. Human Argonaute2 mediates RNA cleavage targeted by miRNAs and siRNAs. Mol Cell. 2004;15(2):185-97. doi: 10.1016/j.molcel.2004.07.007.
8. Liu J, Carmell MA, Rivas FV, Marsden CG, Thomson JM, Song JJ, et al. Argonaute2 is the catalytic engine of mammalian RNAi. Science. 2004;305(5689):1437-41. doi: 10.1126/science.1102513.
9. Potenza N, Papa U, Scaruffi P, Mosca N, Tonini GP, Russo A. A novel splice variant of the human dicer gene is expressed in neuroblastoma cells. FEBS Lett. 2010;584(15):3452-7. doi: S0014-5793(10)00551-X [pii]

10.1016/j.febslet.2010.06.045 [doi].
10. Grelier G, Voirin N, Ay AS, Cox DG, Chabaud S, Treilleux I, et al. Prognostic value of Dicer expression in human breast cancers and association with the mesenchymal phenotype. Br J Cancer. 2009;101(4):673-83. doi: 6605193 [pii]

10.1038/sj.bjc.6605193.
11. Kurzynska-Kokorniak A, Koralewska N, Pokornowska M, Urbanowicz A, Tworak A, Mickiewicz A, et al. The many faces of Dicer: the complexity of the mechanisms regulating Dicer gene expression and enzyme activities. Nucleic Acids Res. 2015;43(9):4365-80. doi: gkv328 [pii]

10.1093/nar/gkv328.
12. Zhang H, Kolb FA, Jaskiewicz L, Westhof E, Filipowicz W. Single processing center models for human Dicer and bacterial RNase III. Cell. 2004;118(1):57-68. doi: 10.1016/j.cell.2004.06.017

S009286740400618X [pii].
13. Macrae IJ, Zhou K, Li F, Repic A, Brooks AN, Cande WZ, et al. Structural basis for double-stranded RNA processing by Dicer. Science. 2006;311(5758):195-8. doi: 311/5758/195 [pii]

10.1126/science.1121638.
14. Macrae IJ, Li F, Zhou K, Cande WZ, Doudna JA. Structure of Dicer and mechanistic implications for RNAi. Cold Spring Harb Symp Quant Biol. 2006;71:73-80. doi: 10.1101/sqb.2006.71.042.
15. Zhang H, Kolb FA, Brondani V, Billy E, Filipowicz W. Human Dicer preferentially cleaves dsRNAs at their termini without a requirement for ATP. EMBO J. 2002;21(21):5875-85.

16. Gan J, Tropea JE, Austin BP, Court DL, Waugh DS, Ji X. Intermediate states of ribonuclease III in complex with double-stranded RNA. Structure. 2005;13(10):1435-42. doi: 10.1016/j.str.2005.06.014.
17. Gan J, Tropea JE, Austin BP, Court DL, Waugh DS, Ji X. Structural insight into the mechanism of double-stranded RNA processing by ribonuclease III. Cell. 2006;124(2):355-66. doi: 10.1016/j.cell.2005.11.034.
18. Koralewska N, Szczepanska A, Ciechanowska K, Wojnicka M, Pokornowska M, Milewski MC, et al. RNA and DNA G-quadruplexes bind to human dicer and inhibit its activity. Cell Mol Life Sci. 2021;78(7):3709-24. doi: 10.1007/s00018-021-03795-w.
19. Tian Y, Simanshu DK, Ma JB, Park JE, Heo I, Kim VN, et al. A Phosphate-Binding Pocket within the Platform-PAZ-Connector Helix Cassette of Human Dicer. Mol Cell. 2014;53(4):606-16. doi: S1097-2765(14)00031-8 [pii]
10.1016/j.molcel.2014.01.003.
20. Ngo MK, Le CT, Nguyen TA. DICER cleavage fidelity is governed by 5'-end binding pockets. Nature. 2026. doi: 10.1038/s41586-026-10211-5.
21. Wu H, Xu H, Miraglia LJ, Crooke ST. Human RNase III is a 160-kDa protein involved in preribosomal RNA processing. J Biol Chem. 2000;275(47):36957-65. doi: 10.1074/jbc.M005494200.
22. Burgers PMJ, Kunkel TA. Eukaryotic DNA Replication Fork. Annu Rev Biochem. 2017;86:417-38. doi: 10.1146/annurev-biochem-061516-044709.
23. Buccheri V, Pasulka J, Malik R, Loubalova Z, Taborska E, Horvat F, et al. Functional canonical RNAi in mice expressing a truncated Dicer isoform and long dsRNA. EMBO Rep. 2024;25(7):2896-913. doi: 10.1038/s44319-024-00148-z.
24. Flemr M, Malik R, Franke V, Nejepinska J, Sedlacek R, Vlahovicek K, et al. A retrotransposon-driven dicer isoform directs endogenous small interfering RNA production in mouse oocytes. Cell. 2013;155(4):807-16. doi: 10.1016/j.cell.2013.10.001.
25. Zapletal D, Taborska E, Pasulka J, Malik R, Kubicek K, Zanova M, et al. Structural and functional basis of mammalian microRNA biogenesis by Dicer. Mol Cell. 2022;82(21):4064-79 e13. doi: 10.1016/j.molcel.2022.10.010.
26. Baldaccini M, Gaucherand L, Chane-Woon-Ming B, Messmer M, Gucciardi F, Pfeffer S. The helicase domain of human Dicer prevents RNAi-independent activation of antiviral and inflammatory pathways. EMBO J. 2024;43(5):806-35. doi: 10.1038/s44318-024-00035-2.
27. Ma E, MacRae IJ, Kirsch JF, Doudna JA. Autoinhibition of human dicer by its internal helicase domain. J Mol Biol. 2008;380(1):237-43. doi: S0022-2836(08)00547-0 [pii]
10.1016/j.jmb.2008.05.005.
28. Ciechanowska K, Szczepanska A, Szpotkowski K, Wojcik K, Urbanowicz A, Kurzynska-Kokorniak A. The human Dicer helicase domain is capable of ATP hydrolysis and single-stranded nucleic acid binding. BMC Biol. 2024;22(1):287. doi: 10.1186/s12915-024-02082-x.
29. Kennedy EM, Whisnant AW, Kornepati AV, Marshall JB, Bogerd HP, Cullen BR. Production of functional small interfering RNAs by an amino-terminal deletion mutant of human Dicer. Proc Natl Acad Sci U S A. 2015;112(50):E6945-54. doi: 10.1073/pnas.1513421112.
30. Poirier EZ, Buck MD, Chakravarty P, Carvalho J, Frederico B, Cardoso A, et al. An isoform of Dicer protects mammalian stem cells against multiple RNA viruses. Science. 2021;373(6551):231-6. doi: 10.1126/science.abg2264.
31. Mosca N, Starega-Roslan J, Castiello F, Russo A, Krzyzosiak WJ, Potenza N. Characterization of a naturally occurring truncated Dicer. Mol Biol Rep. 2015;42(8):1333-40. doi: 10.1007/s11033-015-3878-6.
32. Tang Z, Kang B, Li C, Chen T, Zhang Z. GEPIA2: an enhanced web server for large-scale expression profiling and interactive analysis. Nucleic Acids Res. 2019;47(W1):W556-W60. doi: 10.1093/nar/gkz430.

33. Wojnicka M, Szczepanska A, Kurzynska-Kokorniak A. Unknown Areas of Activity of Human Ribonuclease Dicer: A Putative Deoxyribonuclease Activity. Molecules. 2020;25(6). doi: 10.3390/molecules25061414.
34. Gurtan AM, Lu V, Bhutkar A, Sharp PA. In vivo structure-function analysis of human Dicer reveals directional processing of precursor miRNAs. RNA. 2012;18(6):1116-22. doi: rna.032680.112 [pii]
10.1261/rna.032680.112 [doi].
35. Kurzynska-Kokorniak A, Koralewska N, Tyczewska A, Twardowski T, Figlerowicz M. A New Short Oligonucleotide-Based Strategy for the Precursor-Specific Regulation of microRNA Processing by Dicer. PLoS One. 2013;8(10):e77703. doi: 10.1371/journal.pone.0077703 [doi]
PONE-D-13-24872 [pii].
36. Tyczewska A, Kurzynska-Kokorniak A, Koralewska N, Szopa A, Kietrys AM, Wrzesinski J, et al. Selection of RNA oligonucleotides that can modulate human dicer activity in vitro. Nucleic Acid Ther. 2011;21(5):333-46. doi: 10.1089/nat.2011.0304.
37. Bogerd HP, Whisnant AW, Kennedy EM, Flores O, Cullen BR. Derivation and characterization of Dicer- and microRNA-deficient human cells. RNA. 2014;20(6):923-37. doi: 10.1261/rna.044545.114.
38. Livak KJ, Schmittgen TD. Analysis of relative gene expression data using real-time quantitative PCR and the 2(-Delta Delta C(T)) Method. Methods. 2001;25(4):402-8. doi: 10.1006/meth.2001.1262.
39. Drmanac R, Sparks AB, Callow MJ, Halpern AL, Burns NL, Kermani BG, et al. Human genome sequencing using unchained base reads on self-assembling DNA nanoarrays. Science. 2010;327(5961):78-81. doi: 10.1126/science.1181498.
40. Dobin A, Davis CA, Schlesinger F, Drenkow J, Zaleski C, Jha S, et al. STAR: ultrafast universal RNA-seq aligner. Bioinformatics. 2013;29(1):15-21. doi: 10.1093/bioinformatics/bts635.
41. Liao Y, Smyth GK, Shi W. featureCounts: an efficient general purpose program for assigning sequence reads to genomic features. Bioinformatics. 2014;30(7):923-30. doi: 10.1093/bioinformatics/btt656.
42. Wang L, Wang S, Li W. RSeQC: quality control of RNA-seq experiments. Bioinformatics. 2012;28(16):2184-5. doi: 10.1093/bioinformatics/bts356.
43. Chen Y, Chen L, Lun ATL, Baldoni PL, Smyth GK. edgeR v4: powerful differential analysis of sequencing data with expanded functionality and improved support for small counts and larger datasets. Nucleic Acids Res. 2025;53(2). doi: 10.1093/nar/gkaf018.
44. Rohart F, Gautier B, Singh A, Le Cao KA. mixOmics: An R package for 'omics feature selection and multiple data integration. PLoS Comput Biol. 2017;13(11):e1005752. doi: 10.1371/journal.pcbi.1005752.
45. Abramson J, Adler J, Dunger J, Evans R, Green T, Pritzel A, et al. Accurate structure prediction of biomolecular interactions with AlphaFold 3. Nature. 2024;630(8016):493-500. doi: 10.1038/s41586-024-07487-w.
46. Tauriello G, Waterhouse AM, Haas J, Behringer D, Bienert S, Garello T, et al. ModelArchive: A Deposition Database for Computational Macromolecular Structural Models. J Mol Biol. 2025;437(15):168996. doi: 10.1016/j.jmb.2025.168996.
47. Zhao L, Li R, Shao C, Li P, Liu J, Wang K. 3p21.3 tumor suppressor gene RBM5 inhibits growth of human prostate cancer PC-3 cells through apoptosis. World J Surg Oncol. 2012;10:247. doi: 10.1186/1477-7819-10-247.
48. Ubanako PN, Nweke EE, Nsingwane Z, Monchusi B, Penny C. RBBP6 and cancer: from molecular mechanisms to clinical implications. Front Oncol. 2026;16:1841906. doi: 10.3389/fonc.2026.1841906.
49. Koralewska N, Hoffmann W, Pokornowska M, Milewski M, Lipinska A, Bienkowska-Szewczyk K, et al. How short RNAs impact the human ribonuclease Dicer activity: putative regulatory feedback-loops and other RNA-mediated mechanisms controlling microRNA processing. Acta Biochim Pol. 2016;63(4):773-83. doi: 10.18388/abp.2016_1339.
50. Liu ZM, Wang J, Cheng H, Ke X, Sun L, Zhang QC, et al. Cryo-EM Structure of Human Dicer and Its Complexes with a Pre-miRNA Substrate. Cell. 2018;173(5):1191-+. doi: 10.1016/j.cell.2018.03.080.

51. Wang HW, Noland C, Siridechadilok B, Taylor DW, Ma E, Felderer K, et al. Structural insights into RNA processing by the human RISC-loading complex. Nat Struct Mol Biol. 2009;16(11):1148-53. doi: nsmb.1673 [pii]

10.1038/nsmb.1673.
52. Taylor DW, Ma E, Shigematsu H, Cianfrocco MA, Noland CL, Nagayama K, et al. Substrate-specific structural rearrangements of human Dicer. Nature structural & molecular biology. 2013;20(6):662-70. doi: 10.1038/nsmb.2564.
53. Lau PW, Guiley KZ, De N, Potter CS, Carragher B, MacRae IJ. The molecular architecture of human Dicer. Nat Struct Mol Biol. 2012;19(4):436-40. doi: nsmb.2268 [pii]

10.1038/nsmb.2268.
54. Lau PW, Potter CS, Carragher B, MacRae IJ. Structure of the human Dicer-TRBP complex by electron microscopy. Structure. 2009;17(10):1326-32. doi: S0969-2126(09)00336-0 [pii]

10.1016/j.str.2009.08.013.
55. Liu Z, Wang J, Li G, Wang HW. Structure of precursor microRNA's terminal loop regulates human Dicer's dicing activity by switching DExH/D domain. Protein Cell. 2014. doi: 10.1007/s13238-014-0124-2.
56. Fukagawa T, Nogami M, Yoshikawa M, Ikeno M, Okazaki T, Takami Y, et al. Dicer is essential for formation of the heterochromatin structure in vertebrate cells. Nat Cell Biol. 2004;6(8):784-91. doi: 10.1038/ncb1155

ncb1155 [pii].
57. Gullerova M, Proudfoot NJ. Convergent transcription induces transcriptional gene silencing in fission yeast and mammalian cells. Nat Struct Mol Biol. 2012;19(11):1193-201. doi: nsmb.2392 [pii]

10.1038/nsmb.2392 [doi].
58. Verdel A, Jia S, Gerber S, Sugiyama T, Gygi S, Grewal SI, et al. RNAi-mediated targeting of heterochromatin by the RITS complex. Science. 2004;303(5658):672-6. doi: 10.1126/science.1093686

1093686 [pii].
59. Volpe TA, Kidner C, Hall IM, Teng G, Grewal SI, Martienssen RA. Regulation of heterochromatic silencing and histone H3 lysine-9 methylation by RNAi. Science. 2002;297(5588):1833-7. doi: 10.1126/science.1074973

1074973 [pii].
60. Noma K, Sugiyama T, Cam H, Verdel A, Zofall M, Jia S, et al. RITS acts in cis to promote RNA interference-mediated transcriptional and post-transcriptional silencing. Nat Genet. 2004;36(11):1174-80. doi: ng1452 [pii]

10.1038/ng1452.
61. Burger K, Schlackow M, Potts M, Hester S, Mohammed S, Gullerova M. Nuclear phosphorylated Dicer processes double-stranded RNA in response to DNA damage. J Cell Biol. 2017;216(8):2373-89. doi: 10.1083/jcb.201612131.
62. Kurzynska-Kokorniak A, Pokornowska M, Koralewska N, Hoffmann W, Bienkowska-Szewczyk K, Figlerowicz M. Revealing a new activity of the human Dicer DUF283 domain in vitro. Sci Rep. 2016;6:23989. doi: srep23989 [pii]

10.1038/srep23989.
63. Pokornowska M, Milewski MC, Ciechanowska K, Szczepanska A, Wojnicka M, Radogostowicz Z, et al. The RNA-RNA base pairing potential of human Dicer and Ago2 proteins. Cell Mol Life Sci. 2020;77(16):3231-44. doi: 10.1007/s00018-019-03344-6.
64. Martinez G, Choudury SG, Slotkin RK. tRNA-derived small RNAs target transposable element transcripts. Nucleic Acids Res. 2017;45(9):5142-52. doi: 10.1093/nar/gkx103.

65. Camino LP, Dutta A, Barroso S, Pérez-Calero C, Katz JN, García-Rubio M, et al. DICER ribonuclease removes harmful R-loops. Mol Cell. 2023;83(20):3707-19.e5. doi: 10.1016/j.molcel.2023.09.021.
66. Wojcik K, Krzeminska P, Kurzynska-Kokorniak A. Possible role of human ribonuclease dicer in the regulation of R loops. FEBS Open Bio. 2025. doi: 10.1002/2211-5463.70026.
67. White E, Schlackow M, Kamieniarz-Gdula K, Proudfoot NJ, Gullerova M. Human nuclear Dicer restricts the deleterious accumulation of endogenous double-stranded RNA. Nat Struct Mol Biol. 2014;21(6):552-9. doi: nsmb.2827 [pii]

10.1038/nsmb.2827.
68. Chitale S, Richly H. DICER and ZRF1 contribute to chromatin decondensation during nucleotide excision repair. Nucleic Acids Res. 2017;45(10):5901-12. doi: 10.1093/nar/gkx261.
69. Chitale S, Richly H. DICER- and MMSET-catalyzed H4K20me2 recruits the nucleotide excision repair factor XPA to DNA damage sites. J Cell Biol. 2018;217(2):527-40. doi: 10.1083/jcb.201704028.
70. Di Fazio A, Schlackow M, Pong SK, Alagia A, Gullerova M. Dicer dependent tRNA derived small RNAs promote nascent RNA silencing. Nucleic Acids Res. 2022;50(3):1734-52. doi: 10.1093/nar/gkac022.
71. Lee YY, Lee H, Kim H, Kim VN, Roh SH. Structure of the human DICER-pre-miRNA complex in a dicing state. Nature. 2023;615(7951):331-8. doi: 10.1038/s41586-023-05723-3.
72. Sawh AN, Duchaine TF. A truncated form of dicer tilts the balance of RNA interference pathways. Cell Rep. 2013;4(3):454-63. doi: S2211-1247(13)00360-4 [pii]

10.1016/j.celrep.2013.07.013.
73. Doyle M, Badertscher L, Jaskiewicz L, Guttinger S, Jurado S, Hugenschmidt T, et al. The double-stranded RNA binding domain of human Dicer functions as a nuclear localization signal. RNA. 2013;19(9):1238-52. doi: rna.039255.113 [pii]

10.1261/rna.039255.113 [doi].
74. Drake M, Furuta T, Suen KM, Gonzalez G, Liu B, Kalia A, et al. A Requirement for ERK-Dependent Dicer Phosphorylation in Coordinating Oocyte-to-Embryo Transition in C. elegans. Dev Cell. 2014;31(5):614-28. doi: S1534-5807(14)00721-7 [pii]

10.1016/j.devcel.2014.11.004.
75. Arur S, Ohmachi M, Nayak S, Hayes M, Miranda A, Hay A, et al. Multiple ERK substrates execute single biological processes in Caenorhabditis elegans germ-line development. Proc Natl Acad Sci U S A. 2009;106(12):4776-81. doi: 10.1073/pnas.0812285106.
76. Shen Z, Feng X, Fang Y, Li Y, Li Z, Zhan Y, et al. POTEE drives colorectal cancer development via regulating SPHK1/p65 signaling. Cell Death Dis. 2019;10(11):863. doi: 10.1038/s41419-019-2046-7.
77. Barger CJ, Zhang W, Sharma A, Chee L, James SR, Kufel CN, et al. Expression of the POTE gene family in human ovarian cancer. Sci Rep. 2018;8(1):17136. doi: 10.1038/s41598-018-35567-1.
78. Zhang QM, Shen N, Xie S, Bi SQ, Luo B, Lin YD, et al. MAGED4 expression in glioma and upregulation in glioma cell lines with 5-aza-2'-deoxycytidine treatment. Asian Pac J Cancer Prev. 2014;15(8):3495-501. doi: 10.7314/apjcp.2014.15.8.3495.
79. Uno Y, Kanda M, Sato Y, Shimizu D, Umeda S, Hattori N, et al. Expression, Function, and Prognostic Value of MAGE-D4 Protein in Esophageal Squamous Cell Carcinoma. Anticancer Res. 2019;39(11):6015-23. doi: 10.21873/anticanres.13807.
80. Oya H, Kanda M, Takami H, Hibino S, Shimizu D, Niwa Y, et al. Overexpression of melanoma-associated antigen D4 is an independent prognostic factor in squamous cell carcinoma of the esophagus. Dis Esophagus. 2015;28(2):188-95. doi: 10.1111/dote.12156.
81. Chong CE, Lim KP, Gan CP, Marsh CA, Zain RB, Abraham MT, et al. Over-expression of MAGED4B increases cell migration and growth in oral squamous cell carcinoma and is associated with poor disease outcome. Cancer Lett. 2012;321(1):18-26. doi: 10.1016/j.canlet.2012.03.025.
82. Luo WZ, Li X, Wu XX, Shang YW, Meng DH, Chen YL, et al. MAGED4B is a Poor Prognostic Marker of Stomach Adenocarcinoma and a Potential Therapeutic Target for Stomach Adenocarcinoma Tumorigenesis. Int J Gen Med. 2023;16:1681-93. doi: 10.2147/IJGM.S401507.

83. Chai SJ, Fong SCY, Gan CP, Pua KC, Lim PVH, Lau SH, et al. In vitro evaluation of dual-antigenic PV1 peptide vaccine in head and neck cancer patients. Hum Vaccin Immunother. 2019;15(1):167-78. doi: 10.1080/21645515.2018.1520584.
84. Li A, Zhang W, Xia H, Miao Y, Zhou H, Zhang X, et al. Overexpression of CASS4 promotes invasion in non-small cell lung cancer by activating the AKT signaling pathway and inhibiting E-cadherin expression. Tumour Biol. 2016;37(11):15157-64. doi: 10.1007/s13277-016-5411-5.
85. Gao Y, Zhang X, Wang T, Zhang Y, Wang Q, Hu Y. HNRNPCL1, PRAMEF1, CFAP74, and DFFB: Common Potential Biomarkers for Sporadic and Suspected Lynch Syndrome Endometrial Cancer. Cancer Manag Res. 2020;12:11231-41. doi: 10.2147/CMAR.S262421.
86. Jia J, Han Z, Wang X, Zheng X, Wang S, Cui Y. H2B gene family: A prognostic biomarker and correlates with immune infiltration in glioma. Front Oncol. 2022;12:966817. doi: 10.3389/fonc.2022.966817.
87. Lai PM, Gong X, Chan KM. Roles of Histone H2B, H3 and H4 Variants in Cancer Development and Prognosis. Int J Mol Sci. 2024;25(17). doi: 10.3390/ijms25179699.
88. Pang MYH, Sun X, Ausio J, Ishibashi T. Histone H4 variant, H4G, drives ribosomal RNA transcription and breast cancer cell proliferation by loosening nucleolar chromatin structure. J Cell Physiol. 2020;235(12):9601-8. doi: 10.1002/jcp.29770.
89. Durig J, Bug S, Klein-Hitpass L, Boes T, Jons T, Martin-Subero JI, et al. Combined single nucleotide polymorphism-based genomic mapping and global gene expression profiling identifies novel chromosomal imbalances, mechanisms and candidate genes important in the pathogenesis of T-cell prolymphocytic leukemia with inv(14)(q11q32). Leukemia. 2007;21(10):2153-63. doi: 10.1038/sj.leu.2404877.
90. Baldan F, Mio C, Allegri L, Conzatti K, Toffoletto B, Puppin C, et al. Identification of tumorigenesis-related mRNAs associated with RNA-binding protein HuR in thyroid cancer cells. Oncotarget. 2016;7(39):63388-407. doi: 10.18632/oncotarget.11255.
91. Chervona Y, Costa M. Histone modifications and cancer: biomarkers of prognosis? Am J Cancer Res. 2012;2(5):589-97.
92. Pan M, Luo M, Liu L, Chen Y, Cheng Z, Wang K, et al. EGR1 suppresses HCC growth and aerobic glycolysis by transcriptionally downregulating PFKL. J Exp Clin Cancer Res. 2024;43(1):35. doi: 10.1186/s13046-024-02957-5.
93. Wei LL, Wu XJ, Gong CC, Pei DS. Egr-1 suppresses breast cancer cells proliferation by arresting cell cycle progression via down-regulating CyclinDs. Int J Clin Exp Pathol. 2017;10(10):10212-22.
94. Riedel M, Berthelsen MF, Cai H, Haldrup J, Borre M, Paludan SR, et al. In vivo CRISPR inactivation of Fos promotes prostate cancer progression by altering the associated AP-1 subunit Jun. Oncogene. 2021;40(13):2437-47. doi: 10.1038/s41388-021-01724-6.
95. Shao S, Ju M, Lei J, Lu X, Li H, Wang D, et al. Egr-1 inhibits colon cancer cell proliferation, migration and invasion via regulating CDKL1 at the transcriptional level. Oncol Rep. 2021;46(2). doi: 10.3892/or.2021.8120.
96. Wu F, Zhang J, Jiang Q, Li Q, Li F, Li J, et al. MyoD1 promotes the transcription of BIK and plays an apoptosis-promoting role in the development of gastric cancer. Cell Cycle. 2024;23(5):573-87. doi: 10.1080/15384101.2024.2348344.
97. Cai C, Qin X, Wu Z, Shen Q, Yang W, Zhang S, et al. Inhibitory effect of MyoD on the proliferation of breast cancer cells. Oncol Lett. 2016;11(6):3589-96. doi: 10.3892/ol.2016.4448.
98. Okudela K, Woo T, Mitsui H, Suzuki T, Tajiri M, Sakuma Y, et al. Downregulation of ALDH1A1 expression in non-small cell lung carcinomas--its clinicopathologic and biological significance. Int J Clin Exp Pathol. 2013;6(1):1-12.
99. Ou M, Li S, Tang L. PRDM14: A Potential Target for Cancer Therapy. Curr Cancer Drug Targets. 2018;18(10):945-56. doi: 10.2174/1568009618666180430143055.
100. Sybirna A, Tang WWC, Pierson Smela M, Dietmann S, Gruhn WH, Brosh R, et al. A critical role of PRDM14 in human primordial germ cell fate revealed by inducible degrons. Nat Commun. 2020;11(1):1282. doi: 10.1038/s41467-020-15042-0.

101. Fayzullin A, Sandberg CJ, Spreadbury M, Saberniak BM, Grieg Z, Skaga E, et al. Phenotypic and Expressional Heterogeneity in the Invasive Glioma Cells. Transl Oncol. 2019;12(1):122-33. doi: 10.1016/j.tranon.2018.09.014.
102. Pustchi SE, Avci NG, Akay YM, Akay M. Astrocytes Decreased the Sensitivity of Glioblastoma Cells to Temozolomide and Bay 11-7082. Int J Mol Sci. 2020;21(19). doi: 10.3390/ijms21197154.
103. Restrepo A, Smith CA, Agnihotri S, Shekarforoush M, Kongkham PN, Seol HJ, et al. Epigenetic regulation of glial fibrillary acidic protein by DNA methylation in human malignant gliomas. Neuro Oncol. 2011;13(1):42-50. doi: 10.1093/neuonc/noq145.
104. Yang J, Li Y, Han X, Li T, Li D, Liu Q, et al. Targeting estrogen mediated CYP4F2/CYP4F11-20-HETE metabolic disorder decelerates tumorigenesis in ER+ breast cancer. Biochem Biophys Rep. 2024;38:101706. doi: 10.1016/j.bbrep.2024.101706.
105. Wan S, Pan Q, Yang G, Kuang J, Luo S. Role of CYP4F2 as a novel biomarker regulating malignant phenotypes of liver cancer cells via the Nrf2 signaling axis. Oncol Lett. 2020;20(4):13. doi: 10.3892/ol.2020.11874.
106. Kwon J, Bakhoum SF. The Cytosolic DNA-Sensing cGAS-STING Pathway in Cancer. Cancer Discov. 2020;10(1):26-39. doi: 10.1158/2159-8290.CD-19-0761.
107. Kumar V, Bauer C, Stewart JHt. Cancer cell-specific cGAS/STING Signaling pathway in the era of advancing cancer cell biology. Eur J Cell Biol. 2023;102(3):151338. doi: 10.1016/j.ejcb.2023.151338.
108. Liu FR, Jiang MJ, Mei Z, Lin CJ, Tian L. cGAS-STING signalings potentiate tumor progression via sustaining cancer stemness. Transl Oncol. 2022;20:101404. doi: 10.1016/j.tranon.2022.101404.
109. Wang J, Ding N, Li Y, Cheng H, Wang D, Yang Q, et al. Insulin-like growth factor binding protein 5 (IGFBP5) functions as a tumor suppressor in human melanoma cells. Oncotarget. 2015;6(24):20636-49. doi: 10.18632/oncotarget.4114.
110. Hwang JR, Cho YJ, Lee Y, Park Y, Han HD, Ahn HJ, et al. The C-terminus of IGFBP-5 suppresses tumor growth by inhibiting angiogenesis. Sci Rep. 2016;6:39334. doi: 10.1038/srep39334.
111. Gu S, Zhang R, Gu J, Li X, Lv L, Jiang J, et al. HES5 promotes cellular proliferation of non-small cell lung cancer through STAT3 signaling. Oncol Rep. 2017;37(1):474-82. doi: 10.3892/or.2016.5268.
112. Liu J, Lu WG, Ye F, Cheng XD, Hong D, Hu Y, et al. Hes1/Hes5 gene inhibits differentiation via down-regulating Hash1 and promotes proliferation in cervical carcinoma cells. Int J Gynecol Cancer. 2010;20(7):1109-16. doi: 10.1111/igc.0b013e3181ea74ad.
113. Kuang SQ, Fang Z, Zweidler-McKay PA, Yang H, Wei Y, Gonzalez-Cervantes EA, et al. Epigenetic inactivation of Notch-Hes pathway in human B-cell acute lymphoblastic leukemia. PLoS One. 2013;8(4):e61807. doi: 10.1371/journal.pone.0061807.
114. Li Q, Wu B, Daba M, Gao X, Chen B, Song G, et al. Identification of Calcium Channel-Related Gene P2RX2 for Prognosis and Immune Infiltration in Prostate Cancer. Dis Markers. 2022;2022:8058160. doi: 10.1155/2022/8058160.

Supplementary Files

This is a list of supplementary files associated with this preprint. Click to download.

- SupplementaryTableS1.docx
- SupplementaryTableS10.xlsx
- SupplementaryTableS11.xlsx
- SupplementaryTableS12.xlsx
- SupplementaryTableS13.xlsx
- SupplementaryTableS14.xlsx
- SupplementaryTableS15.xlsx
- SupplementaryTableS16.xlsx
- SupplementaryTableS17.xlsx
- SupplementaryTableS2.xlsx
- SupplementaryTableS3.xlsx
- SupplementaryTableS4.xlsx
- SupplementaryTableS5.xlsx
- SupplementaryTableS6.xlsx
- SupplementaryTableS7.xlsx
- SupplementaryTableS8.xlsx
- SupplementaryTableS9.xlsx
- SupplementaryFigures.pdf
- SupplementaryFilesRawData.pdf
- SupplementaryTables.zip